

NACA RM A54A04

6427

TECH LIBRARY KAFB, NM
0143347

RESEARCH MEMORANDUM

EFFECT OF NOSE SHAPE AND TRAILING-EDGE BLUNTNESS ON
THE AERODYNAMIC CHARACTERISTICS OF AN UNSWEPT
WING OF ASPECT RATIO 3.1, TAPER RATIO 0.4,
AND 3-PERCENT THICKNESS

By John C. Heitmeyer

Ames Aeronautical Laboratory
Moffett Field, Calif.

**NATIONAL ADVISORY COMMITTEE
FOR AERONAUTICS**

WASHINGTON

March 15, 1954

CONFIDENTIAL

Classification cancelled (or changed to) UNCLASSIFIED

By authority of NASA Tech. Pub. Announcement #24
(OFFICER AUTHORIZED TO CHANGE)

By 10 FROSP
NAME AND

[Signature]
GRADE OF OFFICER MAKING CHANGE)

... 28 Mar 61
DATE



NATIONAL ADVISORY COMMITTEE FOR AERONAUTICS

RESEARCH MEMORANDUM

EFFECT OF NOSE SHAPE AND TRAILING-EDGE BLUNTNESS ON
THE AERODYNAMIC CHARACTERISTICS OF AN UNSWEPT
WING OF ASPECT RATIO 3.1, TAPER RATIO 0.4,
AND 3-PERCENT THICKNESS

By John C. Heitmeyer

SUMMARY

The effects of blunting the trailing edge and/or rounding the leading edge upon the lift, drag, and pitching-moment characteristics of a plane tapered wing in combination with a body have been experimentally investigated at Mach numbers ranging from 0.61 to 0.93 and from 1.20 to 1.90. Results indicate that blunting the trailing edge to 0.3 of the maximum airfoil thickness reduced the forward movement of the aerodynamic center, noted for the sharp-trailing-edge sections at high subsonic speeds without, in general, a significant reduction in the maximum lift-drag ratio. At all Mach numbers, blunting the trailing edge increased the minimum drag. Rounding the leading edges of the wings having either the sharp or the blunt trailing edges decreased the minimum drag and, with one exception, increased the maximum lift-drag ratios at subsonic speeds. At supersonic speeds the opposite effects were noted.

INTRODUCTION

It was shown in reference 1 that for unswept wings with sharp trailing edges the forward movement of the aerodynamic center with increasing Mach number at high subsonic speeds was reduced or eliminated if the trailing-edge thickness was made equal to or greater than one-half the maximum thickness of the section. Unfortunately, this improvement in stability characteristics was accompanied by an increase in minimum drag and a decrease in maximum lift-drag ratio. It was suggested, therefore, that in light of the results of reference 2, it might be possible to realize the improved pitching-moment characteristics without the deleterious effects on drag by thickening the trailing edge to less than

one-half the maximum thickness of the section. The present investigation was undertaken, therefore, to determine experimentally the aerodynamic characteristics of the wing-body combination of reference 1, employing the same plane tapered wing of aspect ratio 3.1 with 3-percent-thick, circular-arc, biconvex sections, but modified to have a trailing-edge thickness equal to 0.3 of the maximum airfoil thickness. The present investigation was extended to include also wings having the more conventional round-nose airfoil sections to determine if the aforementioned beneficial effects due to blunting the trailing edge would be realized on wings having round-nose airfoil sections.

The experimental data for the models with wings having sharp trailing edges were obtained from the tabulated results of reference 3. The results for the models with the blunt-trailing-edge wings were obtained during the present investigation and are presented herein.

NOTATION

- a.c. aerodynamic center position, percent \bar{c} from leading edge of \bar{c}
- b wing span
- C_D drag coefficient, $\frac{\text{drag}}{qS}$
- $C_{D_{\min}}$ minimum drag coefficient
- C_L lift coefficient, $\frac{\text{lift}}{qS}$
- C_m pitching-moment coefficient, $\frac{\text{pitching moment}}{qS\bar{c}}$
(Pitching moments were referred to a horizontal axis through the quarter point of the wing mean aerodynamic chord.)
- c local wing chord
- \bar{c} mean aerodynamic chord of wing, $\frac{\int_0^{b/2} c^2 dy}{\int_0^{b/2} c dy}$
- $\frac{dC_L}{d\alpha}$ rate of change of lift coefficient with angle of attack, per deg
(The slope is measured between lift coefficients of -0.2 and +0.2.)

$\frac{L}{D}$	lift-drag ratio
$\left(\frac{L}{D}\right)_{\max}$	maximum lift-drag ratio
h	thickness of the trailing edge
M	free-stream Mach number
q	free-stream dynamic pressure
R	Reynolds number based on the mean aerodynamic chord of the wing
r	radius of body
S	wing area formed by extending the leading and trailing edges to the plane of symmetry
t	maximum wing thickness
x	longitudinal distance from nose of body
y	lateral distance measured perpendicular to plane of symmetry
α	angle of attack of body axis, deg

APPARATUS

The experimental investigation was conducted in the Ames 6- by 6-foot supersonic wind tunnel. In this wind tunnel, the test Mach number can be varied continuously and the stagnation pressure can be regulated to maintain a given test Reynolds number.

The models were mounted on a straight sting in the wind tunnel, the diameter of the sting being about 93 percent of the diameter of the body base. A 4-inch-diameter, four-component, strain-gage balance enclosed within the body of the model measured the aerodynamic forces and moments experienced by the model.

The model and pertinent dimensions are shown in figure 1. The airfoil section of each of the four wings considered in the present investigation is illustrated in figure 2. The sections having a blunt trailing edge were derived by thickening the section at the trailing edge to 0.3 of the maximum thickness and fairing to the biconvex surface by

means of straight lines. The forward half of the round-nose sections was a semiellipse which for the thickness ratios considered closely resembled the NACA 66-003 airfoil section.¹

The solid steel wing of reference 1, having a 3-percent-thick biconvex section, was modified, by the addition of bismuth-tin alloy, to obtain the desired contours for the remaining three wings. With the exception of the aluminum nosepiece, the body was constructed of steel. All exposed surfaces of the wing and body were smooth and polished.

REDUCTION OF DATA

A complete discussion of the methods used to reduce the wind-tunnel data to coefficient form and of the various corrections applied to the data can be found in reference 1. These corrections, which were of the same magnitude for all models, account for the following factors:

1. Induced effects of the tunnel walls at subsonic speeds resulting from lift on the model. The magnitude of these corrections which were added to the uncorrected data were as follows:

$$\Delta\alpha = 0.57 C_L, \text{ deg}$$

$$\Delta C_D = 0.0100 C_L^2$$

2. Change in the velocity of the air stream in the vicinity of the model at subsonic speeds due to constriction of the flow by the tunnel walls. At a Mach number of 0.93 (the maximum subsonic Mach number at which data up to $\pm 4^\circ$ angle of attack could be obtained without choking the wind tunnel) this correction amounted to about a 3-percent increase in the Mach number over that determined from a calibration of the wind tunnel without a model in place.

3. The longitudinal force experienced by the body of the model due to the streamwise variation of static pressure measured in the test section at subsonic and supersonic speeds without a model in place. This correction varied from -0.0007 (at a Mach number of 1.3) to +0.0010 (at a Mach number of 0.93).

It should be noted that the drag coefficients presented herein have been adjusted to represent drag coefficients for which the fuselage base pressure would be equal to the free-stream static pressure.

¹The ordinates of the NACA 66-003 section were obtained by halving the ordinates of the NACA 66-006 section.

Tests of the models having the round-nose airfoils in both an upright and inverted position have indicated that an effective stream angle of about -0.1° exists in the pitch plane of the models at both subsonic and supersonic speeds. The data presented herein have not been corrected for this effect.

RESULTS AND DISCUSSION

The data obtained during the present investigation of two tapered unswept wings with blunt-trailing-edge sections have been tabulated in tables I and II. Comparable data for the wings having a sharp-trailing-edge section have been presented in the tables of reference 3. Analysis of the data from reference 3 showed that the drag data obtained at the lower test Reynolds numbers (1.4 million and 2.4 million) at subsonic speeds exhibited considerable asymmetry between data obtained at positive and negative lift coefficients. At supersonic speeds, the slight asymmetry observed was considerably less than at subsonic speeds and was considered to be within the accuracy of the drag measurements.

As a consequence of the above analysis, only data obtained at the highest test Reynolds number (3.8 million) are presented graphically at both subsonic and supersonic Mach numbers. At supersonic speeds, however, data obtained at a Reynolds number of 2.4 million have also been presented graphically for all models in order to extend or supplement the range of Mach numbers, since power limitation restricted the supersonic Mach number range at the highest test Reynolds number.

Effect of Trailing-Edge Bluntness

Lift and pitching-moment characteristics.— The variations of lift coefficient with angle of attack and of pitching-moment coefficient with lift coefficient for the models under consideration are presented in figures 3 and 4, respectively. The variation with Mach number of the lift-curve slope and position of the aerodynamic center are presented in figures 5 and 6, respectively. The results show that blunting the trailing edge of a sharp-nose airfoil increased the value of lift-curve slope throughout the lift-coefficient range, as shown in figure 3, and the Mach number range, as shown in figure 5. This increase was most evident at subsonic speeds and in the range of lift coefficients, -0.2 to 0.2 (for which the results of fig. 5(a) are applicable), wherein the wing with the biconvex section exhibited low values of lift-curve slope. These small values of lift-curve slope near zero lift have been observed in two-dimensional investigations at subsonic speeds of 6- and 10-percent-thick biconvex sections at Reynolds numbers comparable to those of the

present investigation (refs. 4 and 5). Reference 4 indicates, however, that at Reynolds numbers approaching full scale (18 million), the non-linear variation near zero lift is eliminated and the value of the lift-curve slope is substantially increased. It is believed, therefore, that the benefits indicated in figure 5(a) that result from blunting the trailing edge of the sharp-nose airfoil are optimistic, and that at full-scale Reynolds numbers such benefits at subsonic speeds would resemble more closely those shown for the round-nose section (fig. 5(b)). The increase in lift-curve slope, due to blunting the trailing edge of the wing with the round-nose section, at the high subsonic Mach numbers is attributed to the greater lifting pressures developed over the rear portion of the airfoil, due to the rearward shift of the terminal shocks. This increase in the loading (lifting pressure) near the trailing edge at the high subsonic Mach numbers is indicated also by the more negative pitching-moment coefficients shown in figure 4. At supersonic speeds the observed increase in the value of the lift-curve slope due to blunting the trailing edge of the wing with the sharp-nose airfoil is greater than would be predicted by two-dimensional second-order theory. The reason for this effect is not known at present.

Blunting the wing trailing edge to 0.3 of the maximum thickness of the airfoil for the wings having either a round-nose or sharp-nose airfoil reduced the over-all travel of the aerodynamic center with variation in Mach number (fig. 6). This result was in agreement with that shown by reference 1 for wings with trailing-edge thickness equal to or greater than one-half the maximum thickness.

Drag characteristics.— The variation of the drag coefficient at various lift coefficients with Mach number for the models under consideration is presented in figure 7. Blunting the trailing edge increased the minimum drag of the models with either the sharp-nose or round-nose airfoils, at all test Mach numbers. At subsonic speeds the increment in minimum drag, due to blunting the trailing edge, was about constant for both the sharp-nose airfoil and the round-nose airfoil. However, at supersonic speeds, the variation with Mach number of the increment in minimum drag for the sharp-nose airfoil and the round-nose airfoil was noticeably different. In the former case the increment remained about constant, whereas in the latter case the increment decreased with increasing Mach number. Results of a free-flight investigation (ref. 6) of a wing-body combination, having a plan form similar to that of the model of the present investigation, indicate that at a Reynolds number of about 8.0 million the increment in drag due to blunting the trailing edge of a wing with a 4-percent-thick biconvex airfoil decreases with increasing supersonic Mach number. Thus, it is possible that at higher Reynolds numbers the increment in drag noted for the sharp-nose airfoils would decrease with Mach number in a manner similar to that noted for the round-nose airfoils.

Blunting the trailing edge of the wings, having either the sharp or the round leading edges, in general, reduced the maximum lift-drag ratio only slightly at subsonic speeds (see fig. 8), in spite of the large increase in the minimum drag noted previously. The favorable characteristics of drag due to lift indicated at subsonic speeds are believed to be related to an increase in the base pressure (negative drag) at the blunt trailing edge of the wings with angle of attack. (See ref. 1.) At supersonic speeds, the results of figure 7 indicate that the effects of blunting the trailing edge upon the characteristics of drag due to lift of these wings were influenced by the shape of the leading edge. The characteristics of drag due to lift of the wing with the round leading edge were improved by blunting the trailing edge; as a result, the maximum lift-drag ratios for the round-nose airfoil were not affected (fig. 8). The characteristics of drag due to lift of the wing with the sharp leading edge were not influenced significantly by blunting the trailing edge, with the result that the maximum lift-drag ratios were reduced due to the increase in minimum drag.

Effect of Variation in Trailing-Edge Thickness

The variation of several aerodynamic parameters with trailing-edge thickness parameter h/t for the model having a sharp-nose airfoil, at five selected Mach numbers, is presented in figures 9 and 10. The results presented for thicknesses of one-half and greater were obtained from reference 1.² The data indicate that the value of the lift-curve slope at each Mach number is relatively unaffected by thickening the trailing edge beyond $h/t = 0.3$. Except at a Mach number of 0.91, the position of the aerodynamic center was not influenced by variations in the trailing-edge thickness. At all Mach numbers, the minimum drag increased with increasing value of h/t . The maximum lift-drag ratios are reduced slightly as the trailing edge is thickened from 0 to 0.3 of the maximum section thickness and then are decreased appreciably with further increases in trailing-edge thickness.

Effect of Wing Nose Shape

Lift and pitching-moment characteristics.— The variations of lift coefficient with angle of attack and of pitching-moment coefficient with lift coefficient for the models are presented in figures 11 and 12, respectively. The variation with Mach number of the lift-curve slope and position of the aerodynamic center are presented in figures 13 and 14. With the exception of the lift-curve slopes for the wings with

²Data obtained at subsonic speeds were corrected in the manner described in reference 3.

sharp trailing edges at subsonic speeds, little difference was noted in the lift and pitching-moment characteristics near zero lift for wings with either sharp or round leading edges (see figs. 13 and 14). As mentioned previously, however, the small lift-curve slopes of the wing with a biconvex section at subsonic speeds are believed to be a Reynolds number phenomenon; at full-scale Reynolds number, it would be expected that the lift-curve slope for this wing would be larger and approach that of the wing with the round-nose sharp-trailing-edge section.

At lift coefficients outside the range for which the results of figures 13 and 14 are applicable, -0.2 to 0.2, the most significant effect of rounding the leading edges of these wings occurred at a Mach number of 0.91 (see figs. 11 and 12). For wings with either sharp or blunt trailing edges, rounding the leading edges reduced the lift coefficient at which the wings became neutrally stable by approximately 0.1.

Drag characteristics.- The results of figure 15 indicate that the effects on the minimum drag due to rounding the leading edges of the wings were influenced by Mach number. At Mach numbers above 1.2, the minimum drag coefficients were greater for the models with round leading edges while at subsonic speeds, the opposite effect was obtained. The reduction in minimum drag at subsonic speeds is believed to be related to the larger regions of laminar boundary layer present on the wings with rounded leading edges (see ref. 3). The increase in minimum drag observed at Mach numbers greater than 1.2 is related directly to the higher wave drag associated with the bow wave being detached from the round leading edges.

A comparison of the variation of maximum lift-drag ratio with Mach number (fig. 16) shows that rounding the leading edges of the wings increased the $(L/D)_{\max}$ significantly only at the lower subsonic Mach numbers and decreased the $(L/D)_{\max}$ at supersonic speeds. The increase noted at the lower subsonic Mach numbers was due to both a reduction in minimum drag and in the drag due to lift (see fig. 15). Examination of the results indicates that when the critical Mach number is exceeded, the value of the drag due to lift for the wings with round leading edges approaches that for the wings with sharp leading edges. The effects of rounding the leading edges of the wings on the maximum lift-drag ratio then results primarily from changes in the minimum drag coefficient.

CONCLUSIONS

The present report presents results of a wind-tunnel investigation to determine the effects of blunting the trailing edge and of rounding the leading edge upon the aerodynamic characteristics of a plane tapered wing of aspect ratio 3.1 in combination with a body. For the Mach

numbers considered in the present investigation, 0.61 to 0.93 and 1.20 to 1.90, the following results were obtained:

1. The investigation of the effects of blunting the trailing edge of wings, having either round- or sharp-leading-edge airfoils, to 0.3 of the maximum airfoil thickness showed that:

(a) At high subsonic speeds and at a Reynolds number of 3.8 million, blunting the trailing edge increased the lift-curve slope and reduced the forward movement of the aerodynamic center with Mach number without, in general, an appreciable decrease in the value of the maximum lift-drag ratio.

(b) At all test Mach numbers, blunting the trailing edge increased the minimum drag.

2. The investigation of the effects of variation in the trailing-edge thickness of the wing having a sharp-leading-edge airfoil showed that for the range of Mach numbers considered, there were no aerodynamic benefits to be derived by thickening the trailing edge beyond 0.3 of the maximum airfoil thickness.

3. The investigation of the effects of rounding the leading edge of wings having either a sharp or a blunt trailing edge of 0.3 the maximum section thickness showed that:

(a) Rounding the leading edge reduced the minimum drag and, in general, increased the maximum lift-drag ratio at subsonic speeds while having the opposite effect at supersonic speeds.

(b) Only the lift characteristics of the sharp-trailing-edge airfoil were affected by rounding the leading edge. These effects were, however, confined to data obtained at subsonic speeds and in the vicinity of zero lift.

(c) At all Mach numbers, the pitching-moment characteristics of either the blunt- or sharp-trailing-edge models in the region of zero lift were not influenced by rounding the leading edge. At high subsonic speeds ($M=0.91$) rounding the leading edge reduced the lift coefficient at which the longitudinal stability became neutral.

Ames Aeronautical Laboratory
National Advisory Committee for Aeronautics
Moffett Field, Calif., Jan. 4, 1954

REFERENCES

1. Dugan, Duane W.: Effects of Three Types of Blunt Trailing Edges on the Aerodynamic Characteristics of a Plane Tapered Wing of Aspect Ratio 3.1, With a 3-Percent-Thick Biconvex Section. NACA RM A52E01, 1952.
2. Cleary, Joseph W., and Stevens, George L.: The Effects at Transonic Speeds of Thickening the Trailing Edge of a Wing With a 4-Percent Thick Circular-Arc Airfoil. NACA RM A51J11, 1951.
3. Hall, Charles F.: Lift, Drag, and Pitching-Moment of Low-Aspect-Ratio Wings at Subsonic and Supersonic Speeds. NACA RM A53A30, 1953.
4. Underwood, William J., and Nuber, Robert J.: Two-Dimensional Wind-Tunnel Investigation at High Reynolds Numbers of Two Symmetrical Circular-Arc Airfoil Sections With High-Lift Devices. NACA RM L6K22, 1946.
5. Summers, James L., and Page, William A.: Lift and Moment Characteristics at Subsonic Mach Numbers of Four 10-Percent-Thick Airfoil Sections of Varying Trailing-Edge Thickness. NACA RM A50J09, 1950.
6. Morrow, John D.: Measurements of the Effect of Trailing-Edge Thickness on the Zero-Lift Drag of Thin Low-Aspect-Ratio Wings. NACA RM L50F26, 1950.

TABLE 1.- WIND-TUNNEL DATA FOR AN UNSWEPT WING OF ASPECT RATIO 3.1 WITH 3-PERCENT-THICK, ROUNDED-NOSE, BLUNT-TRAILING-EDGE SECTION

[illegible]

TABLE I.- WIND-TUNNEL DATA FOR AN UNSWEPT WING OF ASPECT RATIO 3.1 WITH 3-PERCENT-THICK, ROUNDED-NOSE, BLUNT-TRAILING-EDGE-SECTION - Concluded

α	C_L	C_D	C_m	α	C_L	C_D	C_m	α	C_L	C_D	C_m	α	C_L	C_D	C_m	α	C_L	C_D	C_m	α	C_L	C_D	C_m	α	C_L	C_D	C_m	α	C_L	C_D	C_m
M=0.93 R=2.4x10 ⁶				M=1.20 R=2.4x10 ⁶				M=1.30 R=2.4x10 ⁶				M=1.50 R=2.4x10 ⁶				M=1.70 R=2.4x10 ⁶				M=1.90 R=2.4x10 ⁶				M=0.93 R=3.8x10 ⁶				M=0.70 R=3.8x10 ⁶			
-0.33	-0.040	0.0095	0.001	-0.23	-0.034	0.0175	0.006	-0.29	-0.029	0.0184	0.005	-0.27	-0.021	0.0175	0.004	-0.27	-0.016	0.0156	0.003	-0.27	-0.016	0.0154	0.003	-0.33	-0.040	0.0095	0.001	-0.23	-0.034	0.0175	0.006
-0.66	-0.065	0.0095	-0.002	-0.46	-0.059	0.0178	0.010	-0.57	-0.052	0.0191	0.009	-0.54	-0.039	0.0177	0.008	-0.56	-0.033	0.0159	0.006	-0.55	-0.029	0.0159	0.006	-0.66	-0.065	0.0095	-0.002	-0.46	-0.059	0.0178	0.010
-0.93	-0.092	0.0103	-0.003	-0.74	-0.103	0.0190	0.016	-0.91	-0.084	0.0204	0.015	-0.86	-0.073	0.0186	0.014	-0.88	-0.069	0.0169	0.012	-0.89	-0.064	0.0169	0.012	-0.93	-0.092	0.0103	-0.003	-0.74	-0.103	0.0190	0.016
-1.22	-0.114	0.0106	-0.005	-1.04	-0.124	0.0209	0.020	-1.22	-0.108	0.0226	0.020	-1.15	-0.099	0.0204	0.019	-1.17	-0.093	0.0189	0.018	-1.09	-0.084	0.0189	0.018	-1.22	-0.114	0.0106	-0.005	-1.04	-0.124	0.0209	0.020
-1.53	-0.132	0.0135	-0.003	-1.39	-0.157	0.0241	0.024	-1.53	-0.145	0.0253	0.024	-1.41	-0.132	0.0234	0.023	-1.43	-0.127	0.0219	0.021	-1.25	-0.117	0.0219	0.021	-1.53	-0.132	0.0135	-0.003	-1.39	-0.157	0.0241	0.024
-2.41	-0.239	0.0169	-0.004	-2.40	-0.261	0.0271	0.029	-2.43	-0.249	0.0283	0.028	-2.29	-0.236	0.0264	0.026	-2.31	-0.231	0.0249	0.024	-2.13	-0.222	0.0249	0.024	-2.41	-0.239	0.0169	-0.004	-2.40	-0.261	0.0271	0.029
-2.96	-0.317	0.0241	-0.005	-3.48	-0.348	0.0309	0.033	-3.49	-0.339	0.0326	0.032	-3.35	-0.327	0.0307	0.030	-3.37	-0.322	0.0292	0.029	-3.20	-0.313	0.0292	0.029	-2.96	-0.317	0.0241	-0.005	-3.48	-0.348	0.0309	0.033
-3.96	-0.395	0.0330	-0.009	-4.56	-0.426	0.0339	0.035	-4.57	-0.417	0.0350	0.035	-4.42	-0.405	0.0331	0.033	-4.44	-0.400	0.0316	0.031	-4.27	-0.391	0.0316	0.031	-3.96	-0.395	0.0330	-0.009	-4.56	-0.426	0.0339	0.035
-4.80	-0.508	0.0444	-0.019	-5.66	-0.539	0.0374	0.040	-5.67	-0.530	0.0385	0.040	-5.52	-0.518	0.0366	0.036	-5.54	-0.513	0.0351	0.035	-5.37	-0.504	0.0351	0.035	-4.80	-0.508	0.0444	-0.019	-5.66	-0.539	0.0374	0.040
-5.25	-0.551	0.0491	-0.025	-6.11	-0.582	0.0419	0.044	-6.12	-0.573	0.0430	0.044	-6.00	-0.561	0.0411	0.041	-6.02	-0.556	0.0396	0.039	-5.85	-0.547	0.0396	0.039	-5.25	-0.551	0.0491	-0.025	-6.11	-0.582	0.0419	0.044
-5.66	-0.590	0.0529	-0.028	-6.56	-0.621	0.0456	0.048	-6.57	-0.612	0.0467	0.048	-6.45	-0.600	0.0448	0.044	-6.47	-0.595	0.0433	0.043	-6.30	-0.586	0.0433	0.043	-5.66	-0.590	0.0529	-0.028	-6.56	-0.621	0.0456	0.048
-5.86	-0.597	0.0529	-0.028	-6.76	-0.628	0.0456	0.048	-6.77	-0.619	0.0467	0.048	-6.65	-0.607	0.0448	0.044	-6.67	-0.602	0.0433	0.043	-6.50	-0.593	0.0433	0.043	-5.86	-0.597	0.0529	-0.028	-6.76	-0.628	0.0456	0.048
-6.17	-0.633	0.0567	-0.031	-7.07	-0.664	0.0493	0.052	-7.08	-0.655	0.0504	0.052	-6.96	-0.643	0.0485	0.048	-6.98	-0.638	0.0470	0.047	-6.81	-0.629	0.0470	0.047	-6.17	-0.633	0.0567	-0.031	-7.07	-0.664	0.0493	0.052
-6.56	-0.672	0.0606	-0.034	-7.46	-0.703	0.0530	0.056	-7.47	-0.694	0.0541	0.056	-7.35	-0.682	0.0522	0.052	-7.37	-0.677	0.0507	0.050	-7.20	-0.668	0.0507	0.050	-6.56	-0.672	0.0606	-0.034	-7.46	-0.703	0.0530	0.056
-6.96	-0.711	0.0645	-0.037	-7.86	-0.742	0.0567	0.060	-7.87	-0.733	0.0578	0.060	-7.75	-0.721	0.0559	0.055	-7.77	-0.716	0.0544	0.054	-7.60	-0.707	0.0544	0.054	-6.96	-0.711	0.0645	-0.037	-7.86	-0.742	0.0567	0.060
-7.35	-0.750	0.0684	-0.040	-8.25	-0.781	0.0604	0.064	-8.26	-0.772	0.0615	0.064	-8.14	-0.760	0.0596	0.059	-8.16	-0.755	0.0581	0.058	-7.99	-0.746	0.0581	0.058	-7.35	-0.750	0.0684	-0.040	-8.25	-0.781	0.0604	0.064
-7.75	-0.789	0.0723	-0.043	-8.65	-0.820	0.0641	0.068	-8.66	-0.811	0.0652	0.068	-8.54	-0.799	0.0633	0.063	-8.56	-0.794	0.0618	0.061	-8.39	-0.785	0.0618	0.061	-7.75	-0.789	0.0723	-0.043	-8.65	-0.820	0.0641	0.068
-8.14	-0.828	0.0762	-0.046	-9.04	-0.859	0.0678	0.072	-9.05	-0.850	0.0689	0.072	-8.93	-0.838	0.0670	0.067	-8.95	-0.833	0.0655	0.065	-8.78	-0.824	0.0655	0.065	-8.14	-0.828	0.0762	-0.046	-9.04	-0.859	0.0678	0.072
-8.54	-0.867	0.0801	-0.049	-9.44	-0.898	0.0715	0.076	-9.45	-0.889	0.0726	0.076	-9.33	-0.877	0.0707	0.070	-9.35	-0.872	0.0692	0.069	-9.18	-0.863	0.0692	0.069	-8.54	-0.867	0.0801	-0.049	-9.44	-0.898	0.0715	0.076
-8.93	-0.906	0.0840	-0.052	-9.83	-0.937	0.0752	0.080	-9.84	-0.928	0.0763	0.080	-9.72	-0.916	0.0744	0.074	-9.74	-0.911	0.0729	0.072	-9.57	-0.902	0.0729	0.072	-8.93	-0.906	0.0840	-0.052	-9.83	-0.937	0.0752	0.080
-9.33	-0.945	0.0879	-0.055	-10.23	-0.976	0.0789	0.084	-10.24	-0.967	0.0799	0.084	-10.12	-0.955	0.0780	0.078	-10.14	-0.950	0.0765	0.076	-9.97	-0.941	0.0765	0.076	-9.33	-0.945	0.0879	-0.055	-10.23	-0.976	0.0789	0.084
-9.72	-0.984	0.0918	-0.058	-10.62	-1.015	0.0826	0.088	-10.63	-1.006	0.0837	0.088	-10.51	-0.994	0.0818	0.081	-10.53	-0.989	0.0803	0.080	-10.36	-0.979	0.0803	0.080	-9.72	-0.984	0.0918	-0.058	-10.62	-1.015	0.0826	0.088
-10.12	-1.023	0.0957	-0.061	-11.02	-1.054	0.0863	0.092	-11.03	-1.045	0.0874	0.092	-10.91	-1.033	0.0855	0.085	-10.93	-1.028	0.0840	0.084	-10.76	-1.018	0.0840	0.084	-10.12	-1.023	0.0957	-0.061	-11.02	-1.054	0.0863	0.092
-10.51	-1.062	0.0996	-0.064	-11.41	-1.093	0.0900	0.096	-11.42	-1.084	0.0911	0.096	-11.30	-1.072	0.0891	0.089	-11.32	-1.067	0.0876	0.087	-11.15	-1.057	0.0876	0.087	-10.51	-1.062	0.0996	-0.064	-11.41	-1.093	0.0900	0.096
-10.91	-1.101	0.1035	-0.067	-11.81	-1.132	0.0937	0.100	-11.82	-1.123	0.0948	0.100	-11.70	-1.111	0.0928	0.092	-11.72	-1.106	0.0913	0.091	-11.55	-1.096	0.0913	0.091	-10.91	-1.101	0.1035	-0.067	-11.81	-1.132	0.0937	0.100
-11.30	-1.140	0.1074	-0.070	-12.20	-1.171	0.0974	0.104	-12.21	-1.162	0.0985	0.104	-12.09	-1.150	0.0965	0.096	-12.11	-1.145	0.0950	0.095	-11.94	-1.135	0.0950	0.095	-11.30	-1.140	0.1074	-0.070	-12.20	-1.171	0.0974	0.104
-11.70	-1.179	0.1113	-0.073	-12.60	-1.210	0.1011	0.108	-12.61	-1.201	0.1022	0.108	-12.49	-1.189	0.1002	0.100	-12.51	-1.184	0.0987	0.098	-12.34	-1.174	0.0987	0.098	-11.70	-1.179	0.1113	-0.073	-12.60	-1.210	0.1011	0.108
-12.09	-1.218	0.1152	-0.076	-13.00	-1.250	0.1049	0.112	-13.01	-1.241	0.1060	0.112	-12.89	-1.229	0.1040	0.104	-12.91	-1.224	0.1025	0.102	-12.74	-1.214	0.1025	0.102	-12.09	-1.218	0.1152	-0.076	-13.00	-1.250	0.1049	0.112
-12.49	-1.257	0.1191	-0.079	-13.40	-1.290	0.1087	0.116	-13.41	-1.281	0.1098	0.116	-13.29	-1.269	0.1078	0.107	-13.31	-1.264	0.1063	0.106	-13.14	-1.254	0.1063	0.106	-12.49	-1.257	0.1191	-0.079	-13.40	-1.290	0.1087	0.112
-12.89	-1.296	0.1230	-0.082	-13.80	-1.330	0.1125	0.120	-13.91	-1.321	0.1136	0.120	-13.79	-1.309	0.1116	0.111	-13.81	-1.304	0.1101	0.110	-13.64	-1.294	0.1101	0.110	-12.89	-1.296	0.1230	-0.082	-13.80	-1.330	0.1125	0.120
-13.29	-1.335	0.1269	-0.085	-14.20	-1.370	0.1163	0.124	-14.31	-1.361	0.1174	0.124	-14.19	-1.349	0.1154	0.115	-14.21	-1.344	0.1139	0.113	-14.04	-1.334	0.1139	0.113	-13.29	-1.335	0.1269	-0.085	-14.20	-1.370	0.1163	0.124
-13.70	-1.374	0.1308	-0.088	-14.60	-1.410	0.1201	0.128	-14.71	-1.401	0.1212	0.128	-14.59	-1.389	0.1192	0.119	-14.61	-1.384	0.1177	0.117	-14.44	-1.374	0.1177	0.117	-13.70	-1.374	0.1308	-0.088	-14.60	-1.410	0.1201	0.124
-14.10	-1.413	0.1347	-0.091	-15.00	-1.450	0.1239	0.132	-15.11	-1.441	0.1250	0.132	-14.99	-1.429	0.1230	0.123	-15.01	-1.424	0.1215	0.121	-14.84	-1.414	0.1215	0.121	-14.10	-1.413	0.1347	-0.091	-15.00	-1.450	0.1239	0.128
-14.51	-1.457	0.1386	-0.094	-15.40	-1.490	0.1277	0.136	-15.51																							

TABLE II.- WIND-TUNNEL DATA FOR AN UNSWEPT WING OF ASPECT RATIO 3.1 WITH 3-PERCENT-THICK, SHARP-NOSE, BLUNT-TRAILING-EDGE SECTION

α	C_L	C_D	C_m	α	C_L	C_D	C_m	α	C_L	C_D	C_m	α	C_L	C_D	C_m	α	C_L	C_D	C_m	α	C_L	C_D	C_m
M=0.61 R=2.4x10 ⁶				M=0.71 R=2.4x10 ⁶				M=0.81 R=2.4x10 ⁶				M=0.91 R=2.4x10 ⁶				M=0.93 R=2.4x10 ⁶				M=1.20 R=2.4x10 ⁶			
-0.31	-0.036	0.0102	0	-0.31	-0.037	0.0103	-0.001	-0.32	-0.039	0.0100	-0.001	-0.33	-0.047	0.0211	-0.001	-0.33	-0.049	0.0112	0.003	-0.30	-0.041	0.0186	0.004
-0.58	-0.075	0.0101	-0.001	-0.59	-0.077	0.0103	-0.002	-0.61	-0.081	0.0097	-0.002	-0.63	-0.089	0.0112	-0.001	-0.63	-0.075	0.0116	0.003	-0.59	-0.066	0.0188	0.007
-1.14	-0.092	0.0107	-0.004	-1.16	-0.097	0.0109	-0.004	-1.20	-0.106	0.0109	-0.004	-1.22	-0.122	0.0123	-0.004	-1.24	-0.103	0.0121	0.002	-1.15	-0.113	0.0203	0.012
-2.26	-0.159	0.0144	-0.008	-2.29	-0.161	0.0149	-0.009	-2.34	-0.200	0.0150	-0.010	-2.41	-0.232	0.0172	-0.013	-2.43	-0.130	0.0129	0.001	-2.26	-0.206	0.0294	0.025
-3.37	-0.246	0.0207	-0.013	-3.40	-0.253	0.0215	-0.013	-3.48	-0.290	0.0224	-0.018	-3.59	-0.329	0.0251	-0.020	-3.63	-0.262	0.0195	0.009	-3.36	-0.299	0.0349	0.035
-4.47	-0.327	0.0298	-0.016	-4.53	-0.349	0.0315	-0.017	-4.64	-0.389	0.0340	-0.025	-4.78	-0.435	0.0383	-0.025	-4.83	-0.356	0.0342	0.007	-4.47	-0.392	0.0453	0.053
-5.52	-0.404	0.0403	-0.020	-5.58	-0.425	0.0428	-0.025	-5.68	-0.468	0.0467	-0.030	-5.80	-0.517	0.0520	-0.030	-5.86	-0.425	0.0414	0.003	-5.52	-0.467	0.0559	0.081
-6.52	-0.480	0.0507	-0.025	-6.58	-0.503	0.0530	-0.030	-6.68	-0.550	0.0579	-0.035	-6.80	-0.601	0.0640	-0.035	-6.86	-0.503	0.0518	0.002	-6.52	-0.543	0.0709	0.104
-7.52	-0.559	0.0610	-0.030	-7.58	-0.583	0.0635	-0.035	-7.68	-0.600	0.0680	-0.040	-7.78	-0.659	0.0740	-0.040	-7.86	-0.586	0.0619	0.001	-7.52	-0.621	0.0859	0.130
-8.52	-0.639	0.0713	-0.035	-8.58	-0.657	0.0740	-0.040	-8.68	-0.700	0.0790	-0.045	-8.78	-0.760	0.0850	-0.045	-8.86	-0.662	0.0719	0.001	-8.52	-0.693	0.0969	0.156
-9.52	-0.719	0.0816	-0.040	-9.58	-0.737	0.0843	-0.045	-9.68	-0.780	0.0890	-0.050	-9.78	-0.840	0.0950	-0.050	-9.86	-0.737	0.0824	0.001	-9.52	-0.765	0.1079	0.182
-10.52	-0.799	0.0919	-0.045	-10.58	-0.817	0.0946	-0.050	-10.68	-0.860	0.1000	-0.055	-10.78	-0.920	0.1060	-0.055	-10.86	-0.817	0.0924	0.001	-10.52	-0.837	0.1199	0.208
-11.52	-0.879	0.1022	-0.050	-11.58	-0.895	0.1073	-0.055	-11.68	-0.940	0.1130	-0.060	-11.78	-1.000	0.1190	-0.060	-11.86	-0.895	0.1049	0.001	-11.52	-0.917	0.1329	0.234
-12.52	-0.959	0.1125	-0.055	-12.58	-0.971	0.1174	-0.060	-12.68	-1.000	0.1240	-0.065	-12.78	-1.060	0.1300	-0.065	-12.86	-0.971	0.1169	0.001	-12.52	-0.993	0.1459	0.260
-13.52	-1.039	0.1228	-0.060	-13.58	-1.047	0.1273	-0.065	-13.68	-1.060	0.1360	-0.070	-13.78	-1.120	0.1360	-0.070	-13.86	-1.047	0.1284	0.001	-13.52	-1.065	0.1579	0.286
-14.52	-1.119	0.1331	-0.065	-14.58	-1.127	0.1374	-0.070	-14.68	-1.080	0.1460	-0.075	-14.78	-1.180	0.1460	-0.075	-14.86	-1.119	0.1399	0.001	-14.52	-1.143	0.1699	0.312
-15.52	-1.199	0.1434	-0.070	-15.58	-1.207	0.1477	-0.075	-15.68	-1.100	0.1540	-0.080	-15.78	-1.240	0.1540	-0.080	-15.86	-1.199	0.1514	0.001	-15.52	-1.217	0.1819	0.338
-16.52	-1.279	0.1537	-0.075	-16.58	-1.285	0.1579	-0.080	-16.68	-1.120	0.1620	-0.085	-16.78	-1.280	0.1620	-0.085	-16.86	-1.279	0.1634	0.001	-16.52	-1.295	0.1939	0.364
-17.52	-1.359	0.1640	-0.080	-17.58	-1.363	0.1674	-0.085	-17.68	-1.140	0.1700	-0.090	-17.78	-1.380	0.1700	-0.090	-17.86	-1.359	0.1749	0.001	-17.52	-1.371	0.2039	0.390
-18.52	-1.439	0.1743	-0.085	-18.58	-1.443	0.1769	-0.090	-18.68	-1.160	0.1780	-0.095	-18.78	-1.380	0.1780	-0.095	-18.86	-1.439	0.1849	0.001	-18.52	-1.423	0.2139	0.416
-19.52	-1.519	0.1846	-0.090	-19.58	-1.523	0.1864	-0.095	-19.68	-1.180	0.1800	-0.100	-19.78	-1.380	0.1800	-0.100	-19.86	-1.519	0.1949	0.001	-19.52	-1.483	0.2239	0.442
-20.52	-1.599	0.1949	-0.095	-20.58	-1.603	0.1967	-0.100	-20.68	-1.200	0.1900	-0.105	-20.78	-1.380	0.1900	-0.105	-20.86	-1.599	0.2049	0.001	-20.52	-1.557	0.2339	0.468
-21.52	-1.679	0.2052	-0.100	-21.58	-1.687	0.2084	-0.105	-21.68	-1.220	0.2000	-0.110	-21.78	-1.380	0.2000	-0.110	-21.86	-1.679	0.2149	0.001	-21.52	-1.631	0.2439	0.494
-22.52	-1.759	0.2155	-0.105	-22.58	-1.761	0.2190	-0.110	-22.68	-1.240	0.2100	-0.115	-22.78	-1.380	0.2100	-0.115	-22.86	-1.759	0.2249	0.001	-22.52	-1.703	0.2539	0.520
-23.52	-1.839	0.2258	-0.110	-23.58	-1.843	0.2290	-0.115	-23.68	-1.260	0.2200	-0.120	-23.78	-1.380	0.2200	-0.120	-23.86	-1.839	0.2349	0.001	-23.52	-1.777	0.2639	0.546
-24.52	-1.919	0.2361	-0.115	-24.58	-1.923	0.2370	-0.120	-24.68	-1.280	0.2300	-0.125	-24.78	-1.380	0.2300	-0.125	-24.86	-1.919	0.2449	0.001	-24.52	-1.851	0.2739	0.572
-25.52	-1.999	0.2464	-0.120	-25.58	-2.003	0.2479	-0.125	-25.68	-1.300	0.2400	-0.130	-25.78	-1.380	0.2400	-0.130	-25.86	-1.999	0.2549	0.001	-25.52	-1.925	0.2839	0.598
-26.52	-2.079	0.2567	-0.125	-26.58	-2.083	0.2584	-0.130	-26.68	-1.320	0.2500	-0.135	-26.78	-1.380	0.2500	-0.135	-26.86	-2.079	0.2649	0.001	-26.52	-2.000	0.2939	0.624
-27.52	-2.159	0.2670	-0.130	-27.58	-2.163	0.2690	-0.135	-27.68	-1.340	0.2600	-0.140	-27.78	-1.380	0.2600	-0.140	-27.86	-2.159	0.2749	0.001	-27.52	-2.075	0.3039	0.650
-28.52	-2.239	0.2773	-0.135	-28.58	-2.243	0.2790	-0.140	-28.68	-1.360	0.2700	-0.145	-28.78	-1.380	0.2700	-0.145	-28.86	-2.239	0.2849	0.001	-28.52	-2.150	0.3139	0.676
-29.52	-2.319	0.2876	-0.140	-29.58	-2.323	0.2890	-0.145	-29.68	-1.380	0.2800	-0.150	-29.78	-1.380	0.2800	-0.150	-29.86	-2.319	0.2949	0.001	-29.52	-2.225	0.3239	0.702
-30.52	-2.399	0.2979	-0.145	-30.58	-2.403	0.2990	-0.150	-30.68	-1.400	0.2900	-0.155	-30.78	-1.380	0.2900	-0.155	-30.86	-2.399	0.3049	0.001	-30.52	-2.300	0.3339	0.728
-31.52	-2.479	0.3082	-0.150	-31.58	-2.483	0.3100	-0.155	-31.68	-1.420	0.3000	-0.160	-31.78	-1.380	0.3000	-0.160	-31.86	-2.479	0.3149	0.001	-31.52	-2.375	0.3439	0.754
-32.52	-2.559	0.3185	-0.155	-32.58	-2.563	0.3200	-0.160	-32.68	-1.440	0.3100	-0.165	-32.78	-1.380	0.3100	-0.165	-32.86	-2.559	0.3249	0.001	-32.52	-2.450	0.3539	0.780
-33.52	-2.639	0.3288	-0.160	-33.58	-2.643	0.3300	-0.165	-33.68	-1.460	0.3200	-0.170	-33.78	-1.380	0.3200	-0.170	-33.86	-2.639	0.3349	0.001	-33.52	-2.525	0.3639	0.806
-34.52	-2.719	0.3391	-0.165	-34.58	-2.723	0.3400	-0.170	-34.68	-1.480	0.3300	-0.175	-34.78	-1.380	0.3300	-0.175	-34.86	-2.719	0.3449	0.001	-34.52	-2.600	0.3739	0.832
-35.52	-2.799	0.3494	-0.170	-35.58	-2.803	0.3500	-0.175	-35.68	-1.500	0.3400	-0.180	-35.78	-1.380	0.3400	-0.180	-35.86	-2.799	0.3549	0.001	-35.52	-2.675	0.3839	0.858
-36.52	-2.879	0.3597	-0.175	-36.58	-2.883	0.3600	-0.180	-36.68	-1.520	0.3500	-0.185	-36.78	-1.380	0.3500	-0.185	-36.86	-2.879	0.3649	0.001	-36.52	-2.750	0.3939	0.884
-37.52	-2.959	0.3699	-0.180	-37.58	-2.963	0.3700	-0.185	-37.68	-1.540	0.3600	-0.190	-37.78	-1.380	0.3600	-0.190	-37.86	-2.959	0.3749	0.001	-37.52	-2.825	0.4039	0.910
-38.52	-3.039	0.3802	-0.185	-38.58	-3.043	0.3800	-0.190	-38.68	-1.560	0.3700	-0.195	-38.78	-1.380	0.3700	-0.195	-38.86	-3.039	0.3849	0.001	-38.52	-2.900	0.4139	0.936
-39.52	-3.119	0.3905	-0.190	-39.58	-3.123	0.3900	-0.195	-39.68	-1.580	0.3800	-0.200	-39.78	-1.380	0.3800	-0.200	-39.86	-3.119	0.3949	0.001	-39.52	-2.975	0.4239	0.962
-40.52	-3.199	0.4008	-0.195	-40.58	-3.203	0.4000	-0.200	-40.68	-1.600	0.3900	-0.205	-40.78	-1.380	0.3900	-0.205	-40.86	-3.199	0.4049	0.001	-40.52	-3.050	0.4339	0.988
-41.52	-3.279	0.4111	-0.200	-41.58	-3.283	0.4100	-0.205	-41.68	-1.620	0.4000	-0.210	-41.78	-1.380	0.4000	-0.210	-41.86	-3.279	0.4149	0.001	-41.52	-3.125	0.4439	1.014
-42.52	-3.359	0.4214	-0.205	-42.58	-3.363	0.4200	-0.210	-42.68	-1.640	0.4100	-0.215	-42.78	-1.380	0.4100	-0.215	-42.86							

~~CONFIDENTIAL~~

NACA RM A54AO4

~~CONFIDENTIAL~~

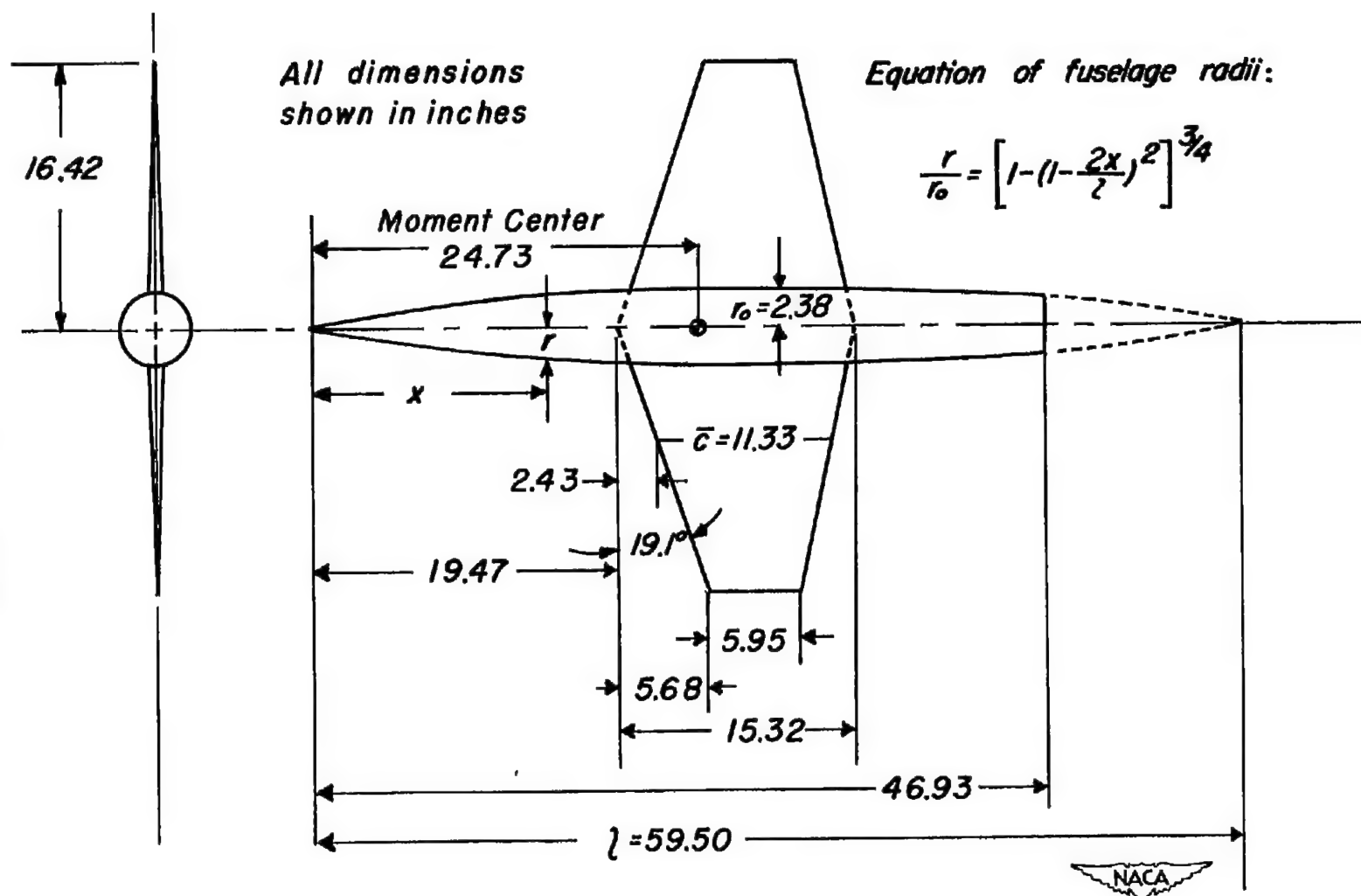
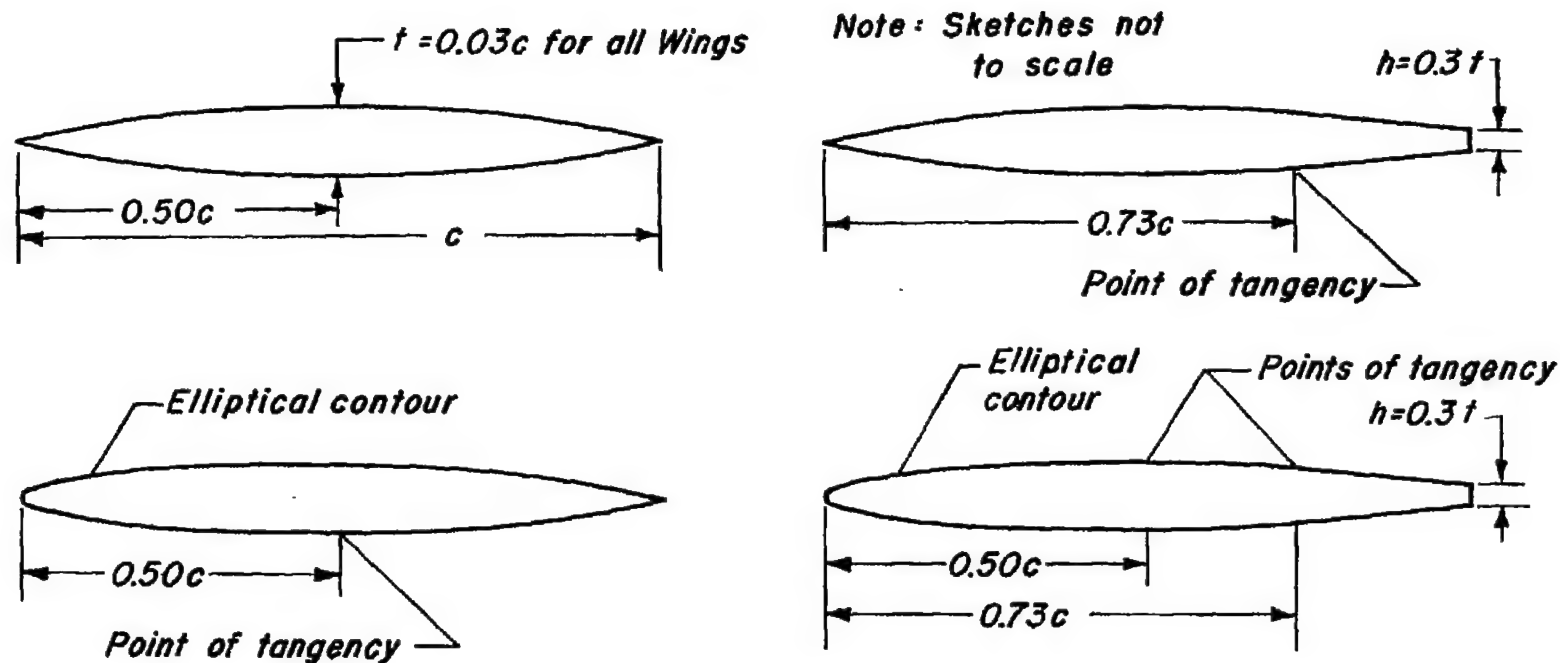
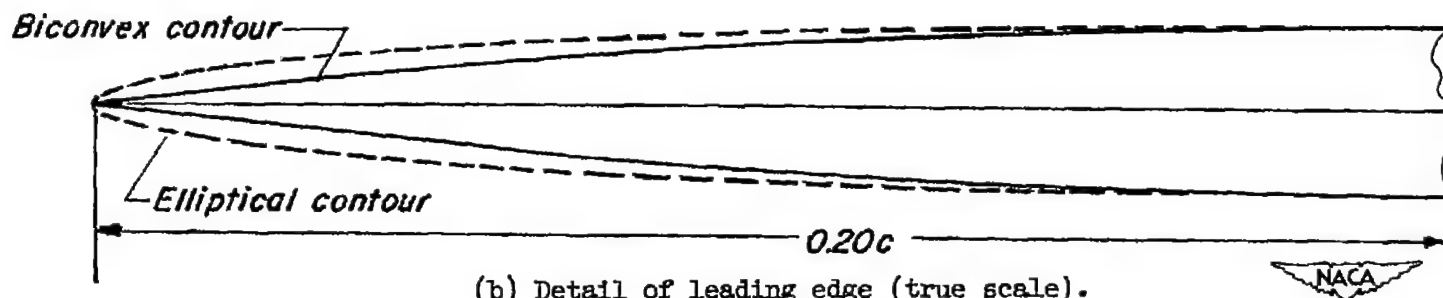


Figure 1.- Plan view and front view of model.

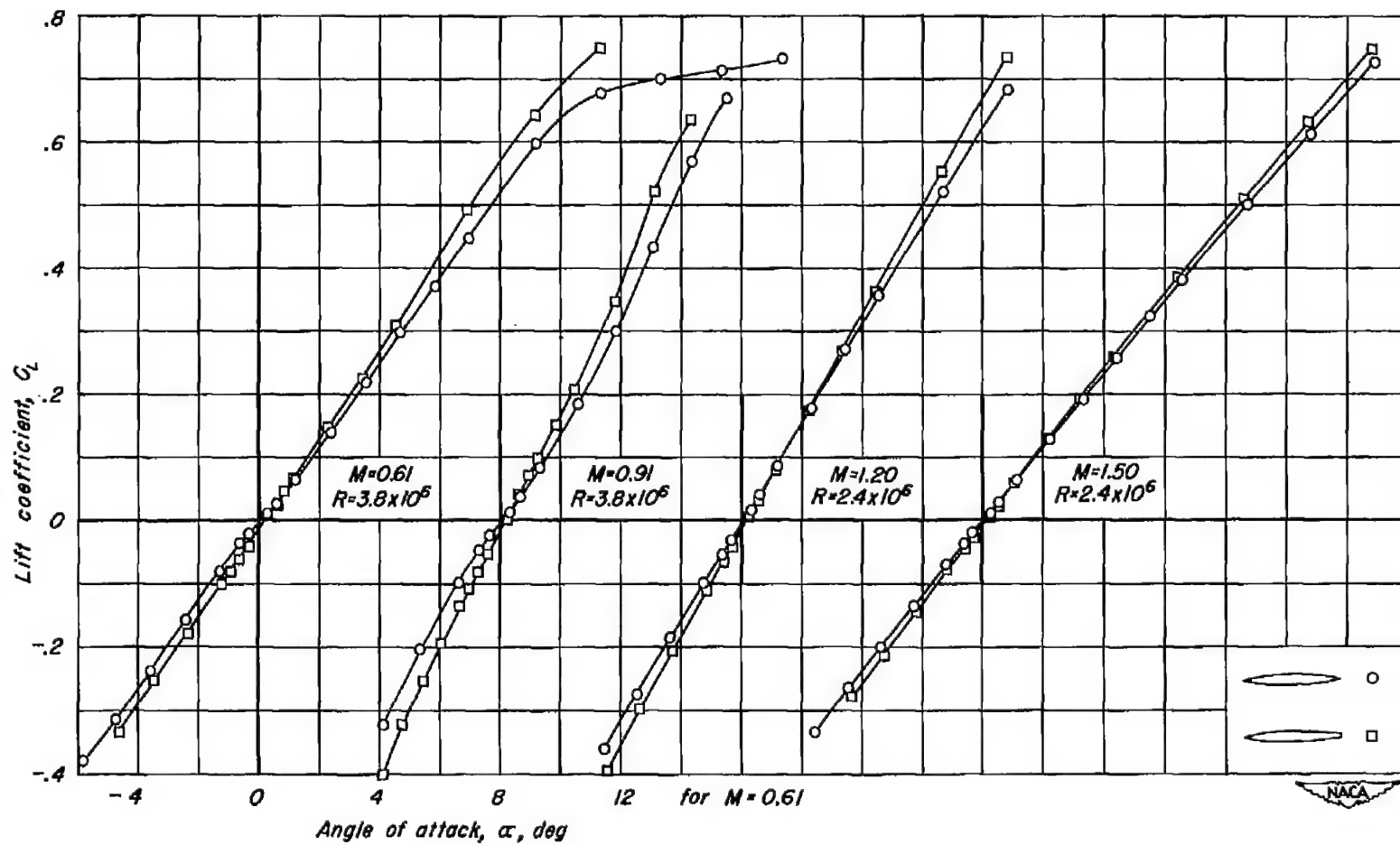


(a) Sketches of airfoil section of various wings.



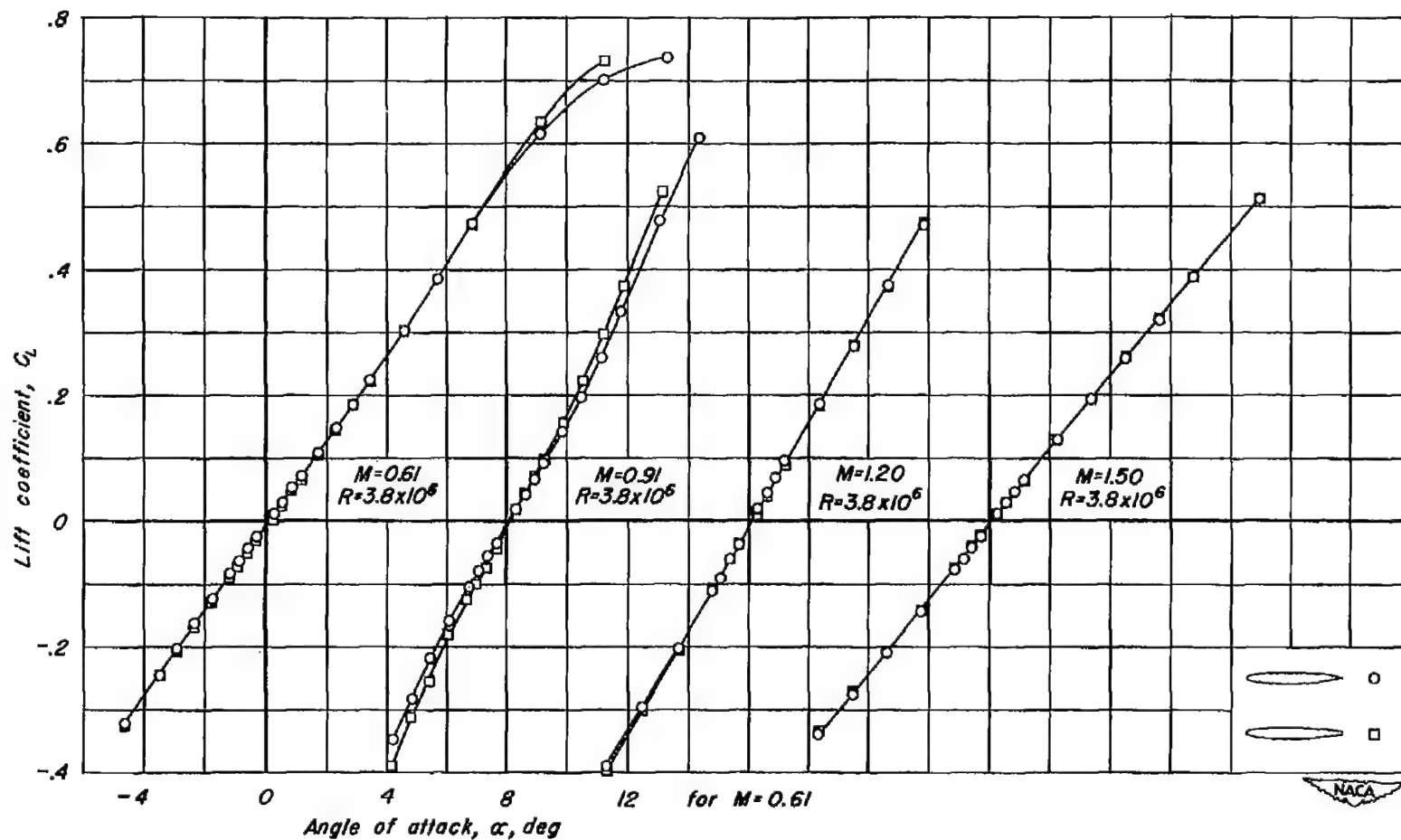
(b) Detail of leading edge (true scale).

Figure 2.- Sections of various wings.



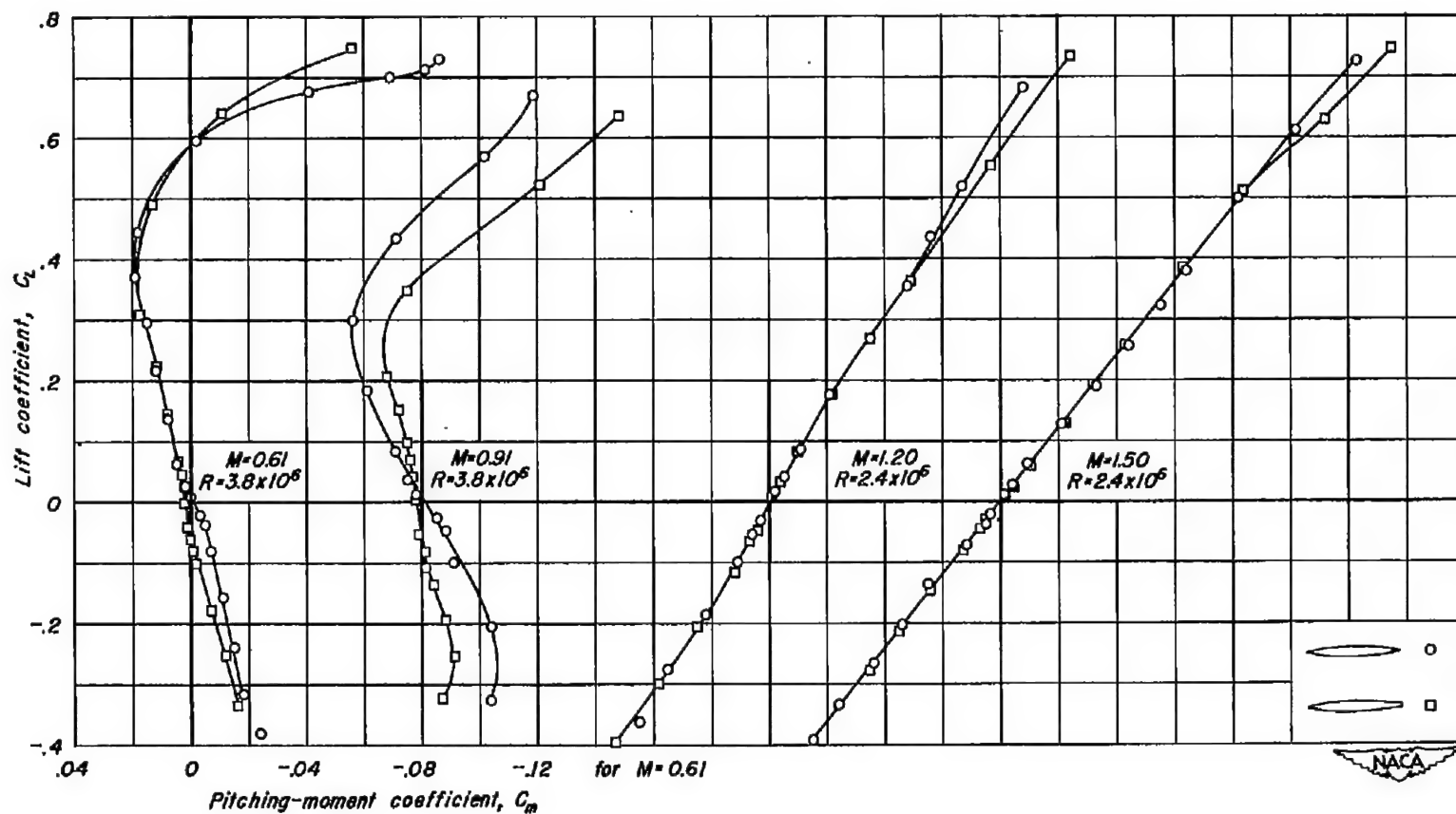
(a) Sharp-nose airfoils.

Figure 3.- Effect of blunt trailing edge ($h/t = 0.3$) on the variation of lift coefficient with angle of attack at various Mach numbers.



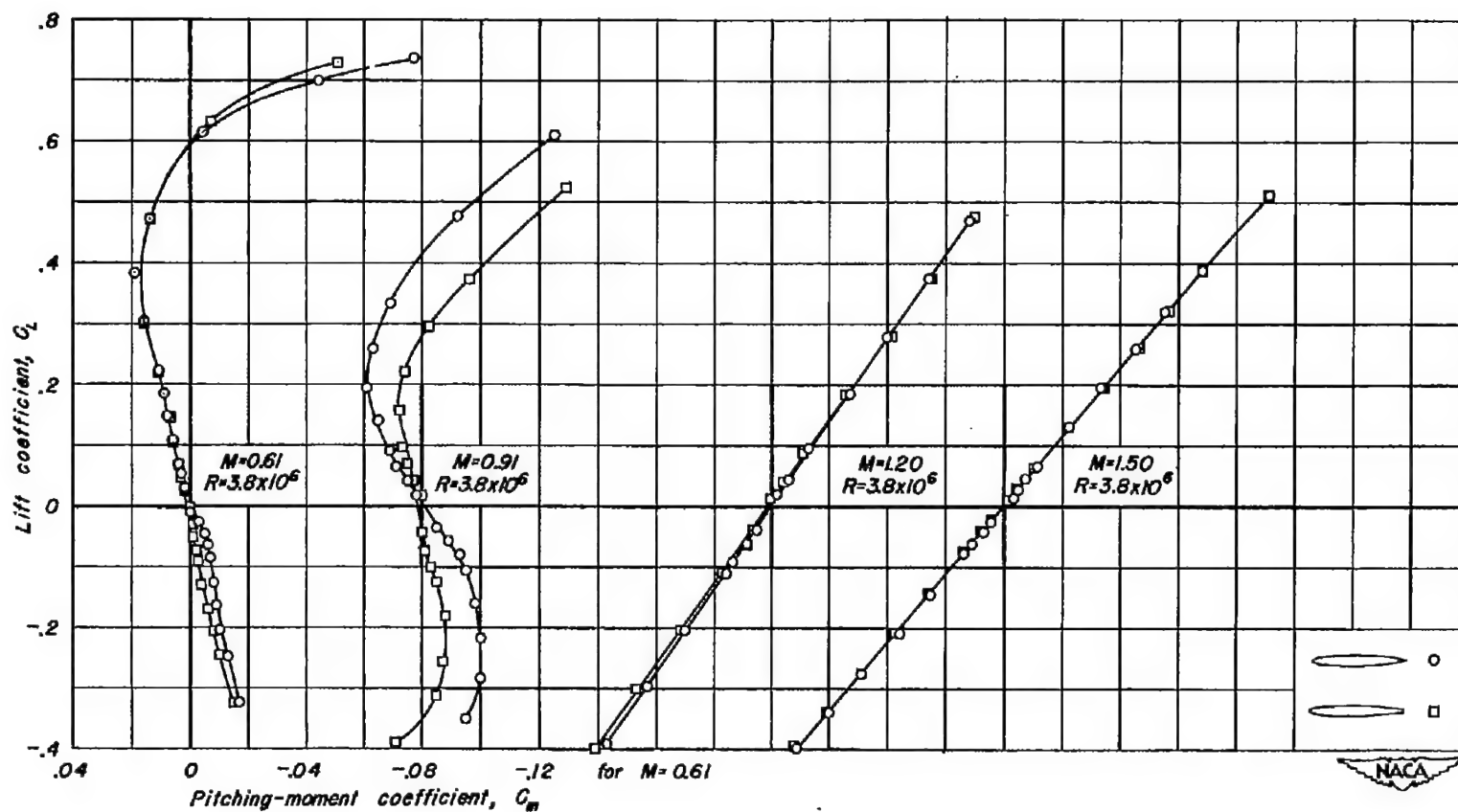
(b) Round-nose airfoils.

Figure 3.- Concluded.



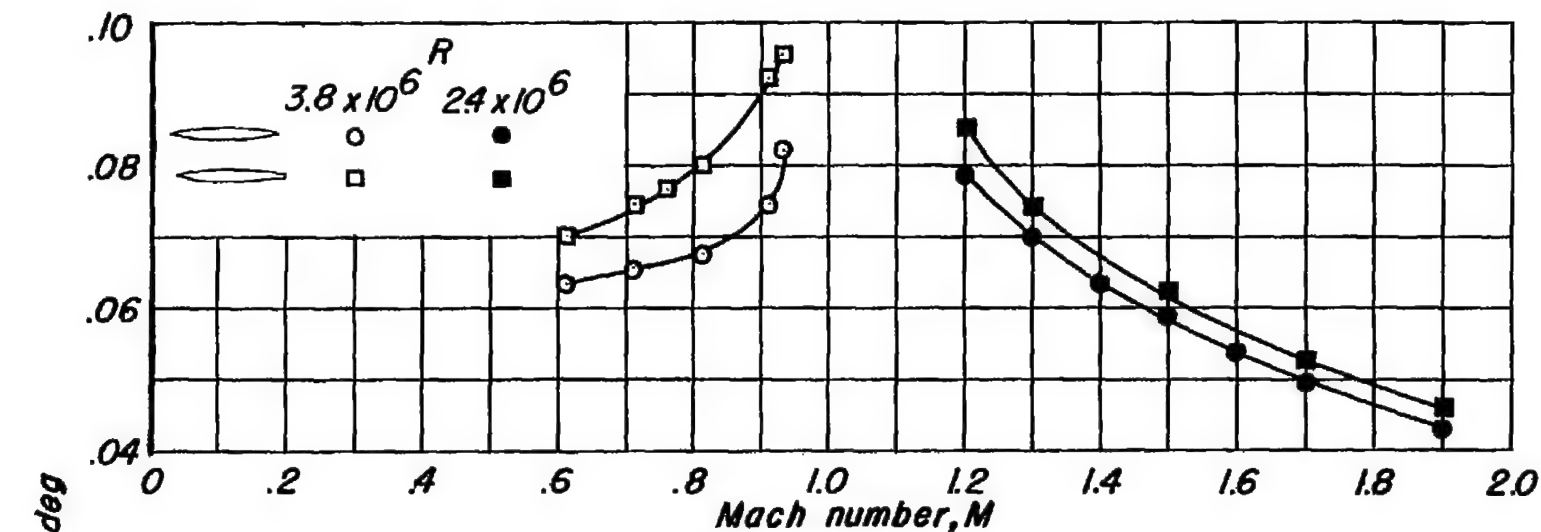
(a) Sharp-nose airfoils.

Figure 4.- Effect of blunt trailing edge ($h/t = 0.3$) on the variation of pitching-moment coefficient with lift coefficient at various Mach numbers.

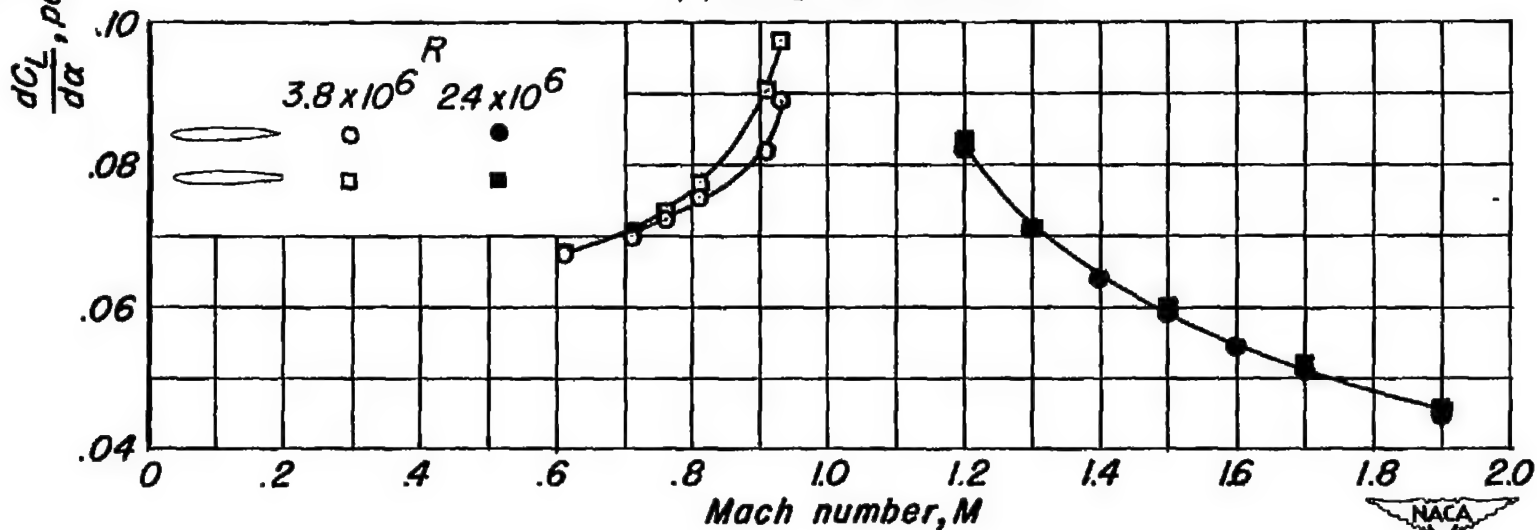


(b) Round-nose airfoils.

Figure 4.- Concluded.

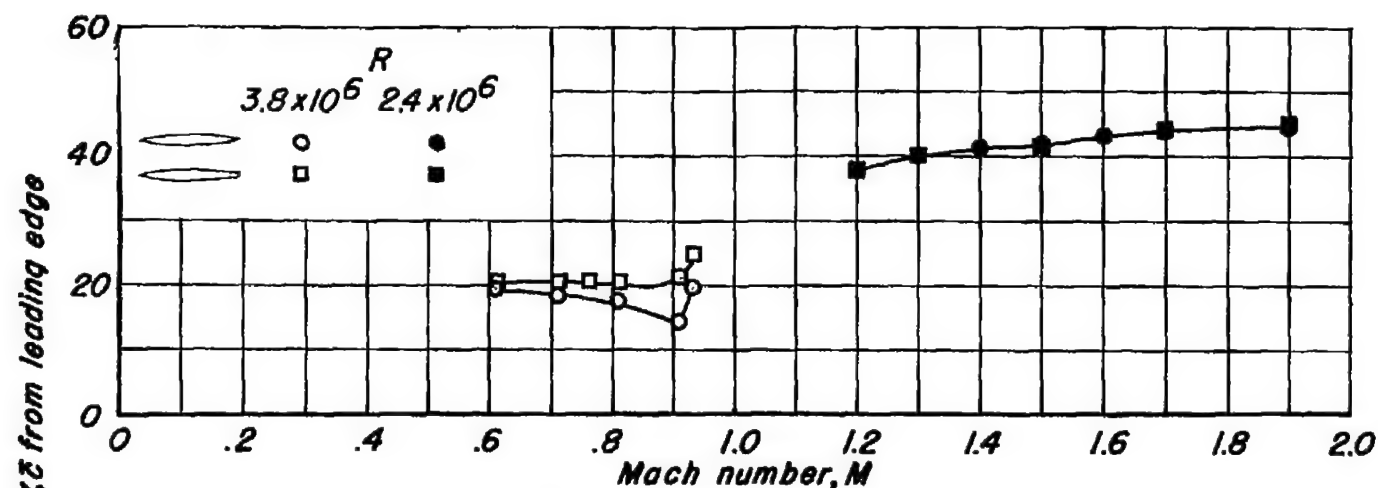


(a) Sharp-nose airfoils.

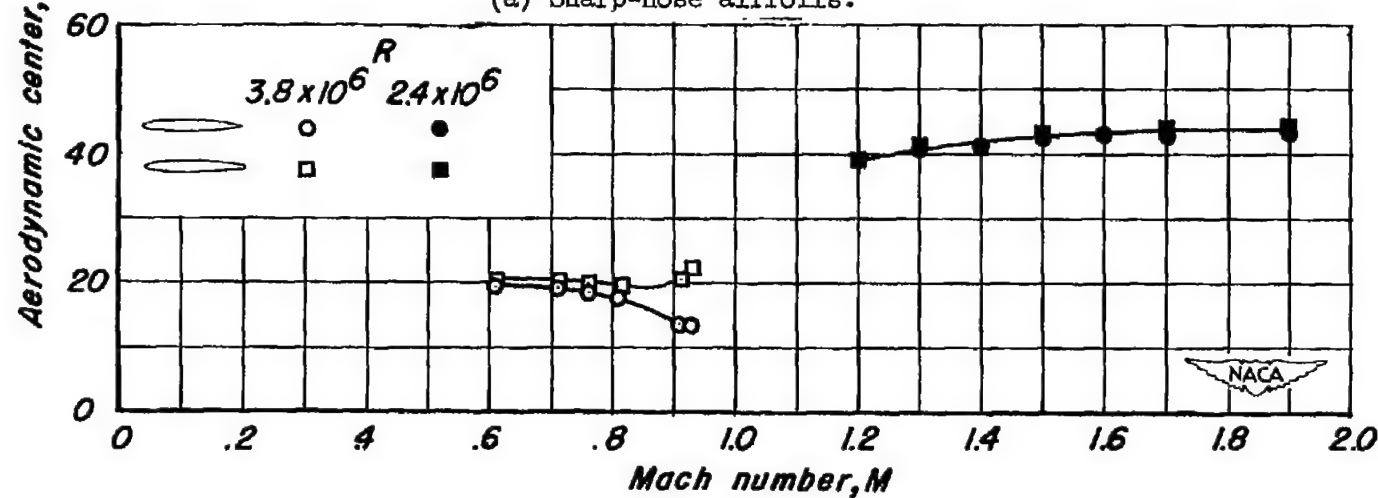


(b) Round-nose airfoils.

Figure 5.- Effect of blunt trailing edge ($h/t = 0.3$) on the variation of lift-curve slope with Mach number.

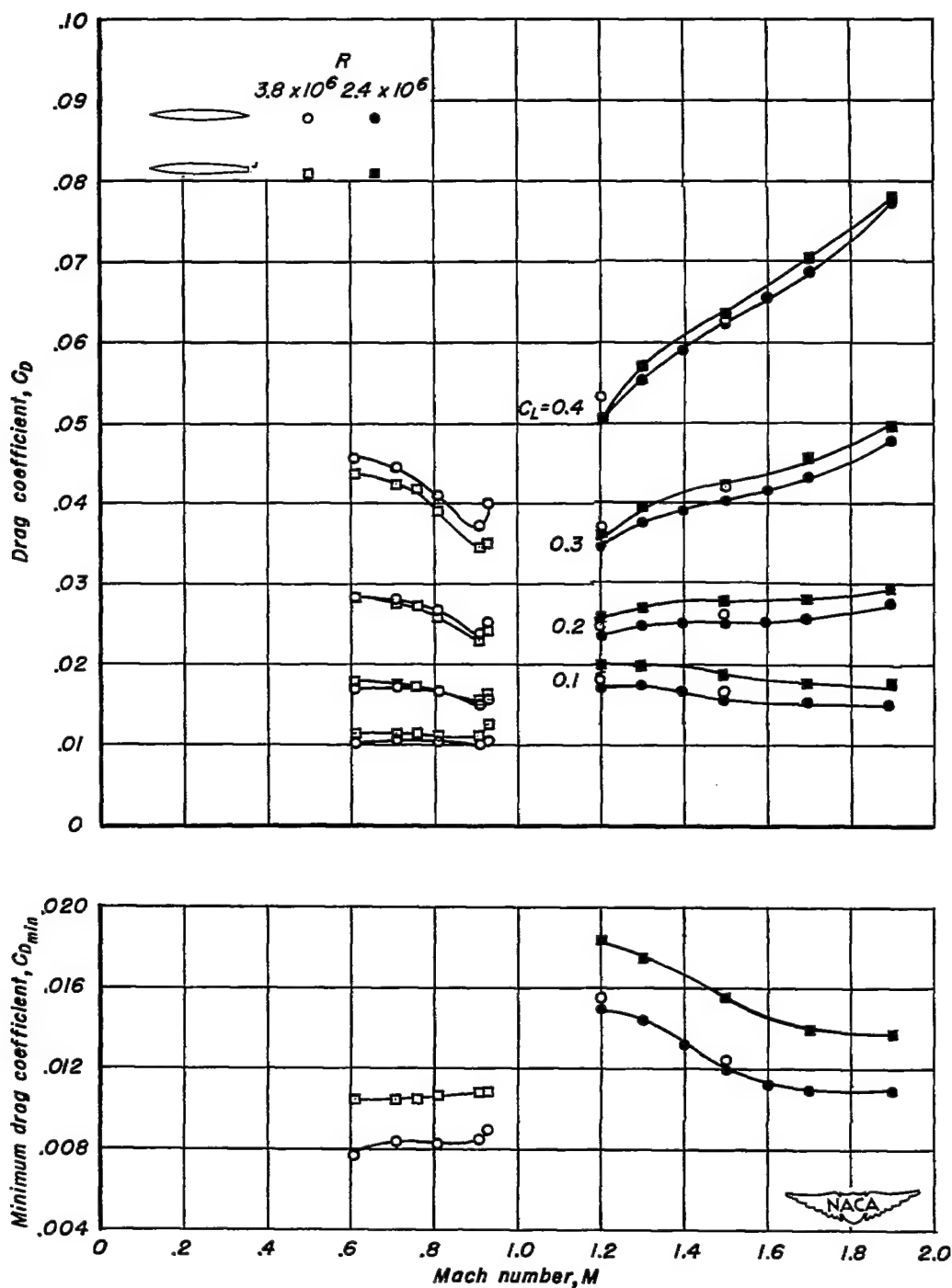


(a) Sharp-nose airfoils.



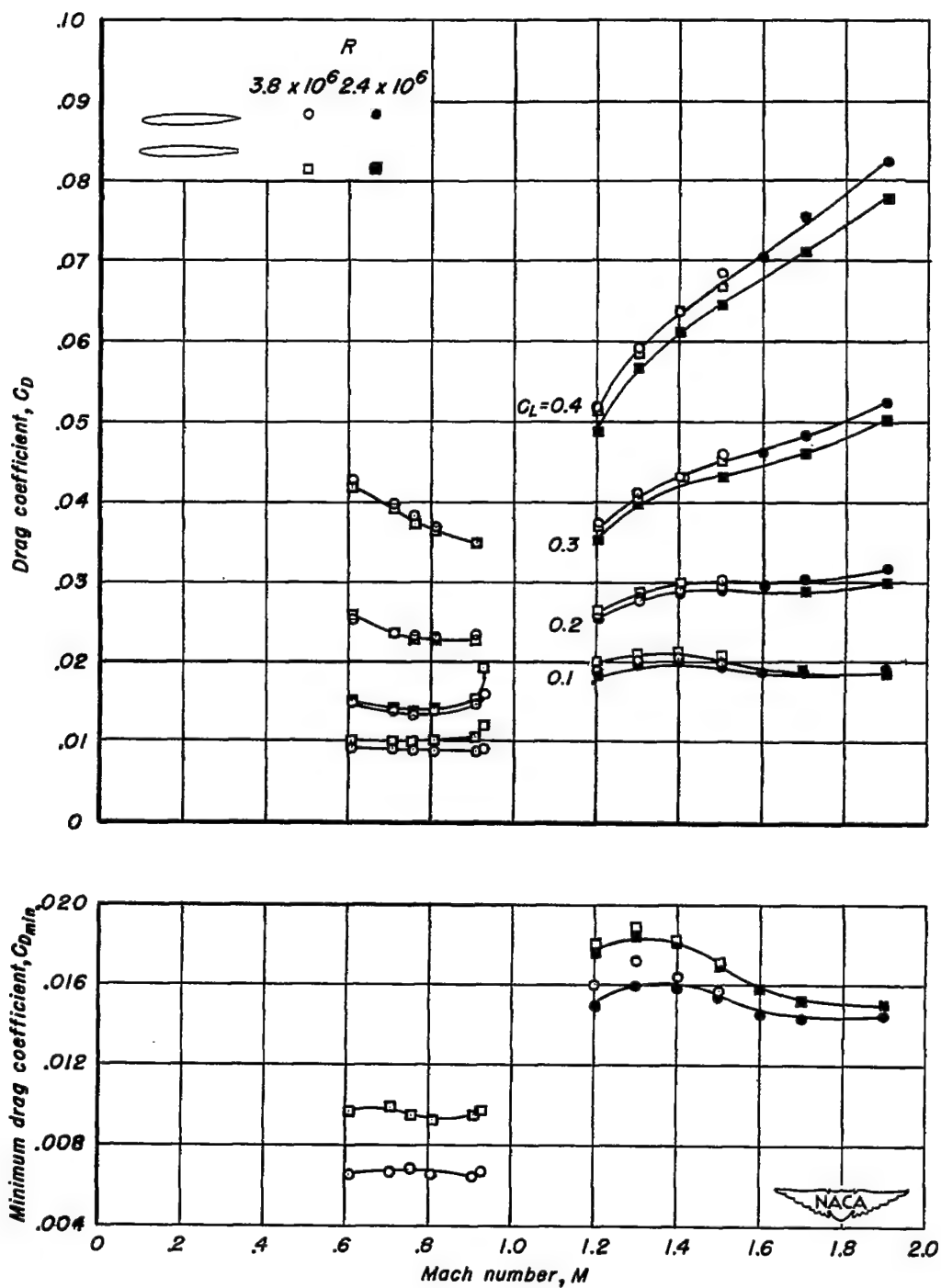
(b) Round-nose airfoils.

Figure 6.- Effect of blunt trailing edge ($h/t = 0.3$) on the variation of aerodynamic center with Mach number.



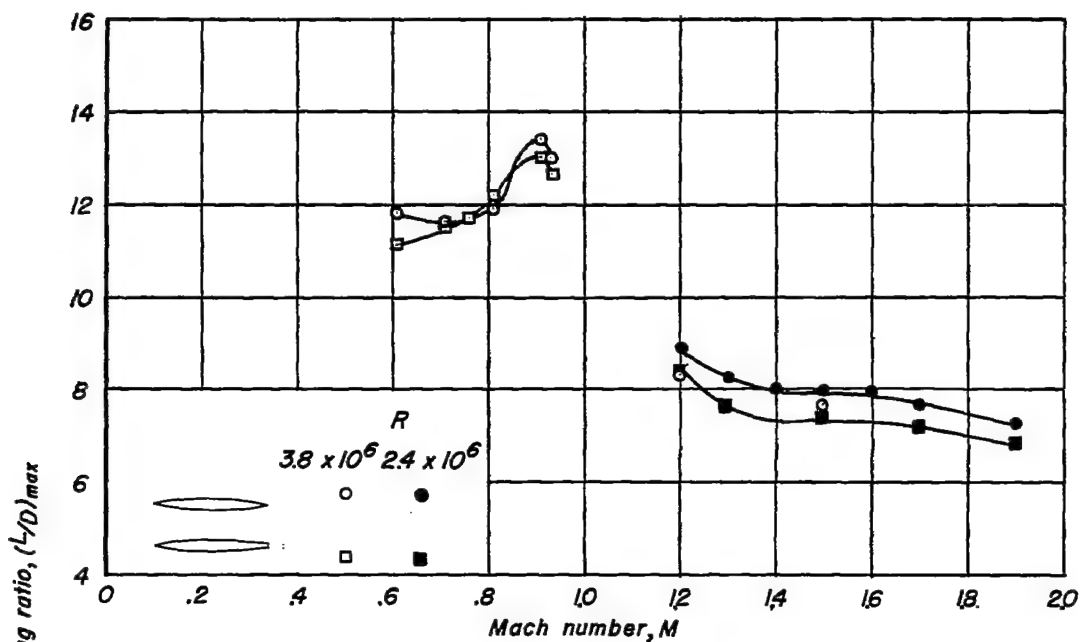
(a) Sharp-nose airfoils.

Figure 7.- Effect of blunt trailing edge ($h/t = 0.3$) on the variation of drag coefficient at various lift coefficients with Mach number.

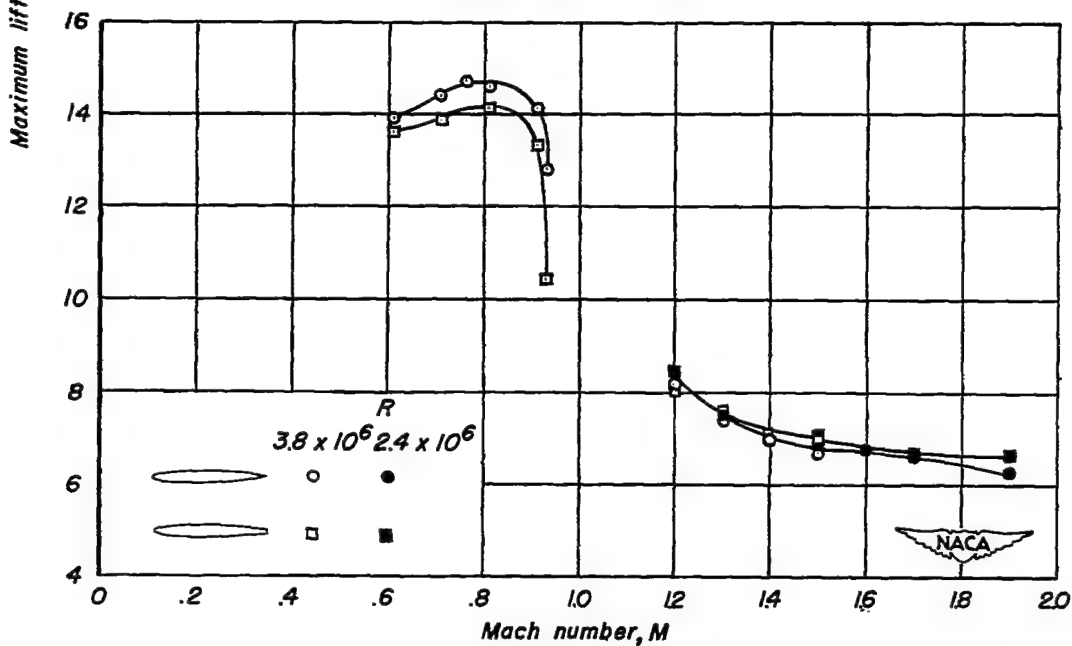


(b) Round-nose airfoils.

Figure 7.- Concluded.



(a) Sharp-nose airfoils.



(b) Round-nose airfoils.

Figure 8.- Effect of blunt trailing edge ($h/t = 0.3$) on the variation of maximum lift-drag ratio with Mach number.

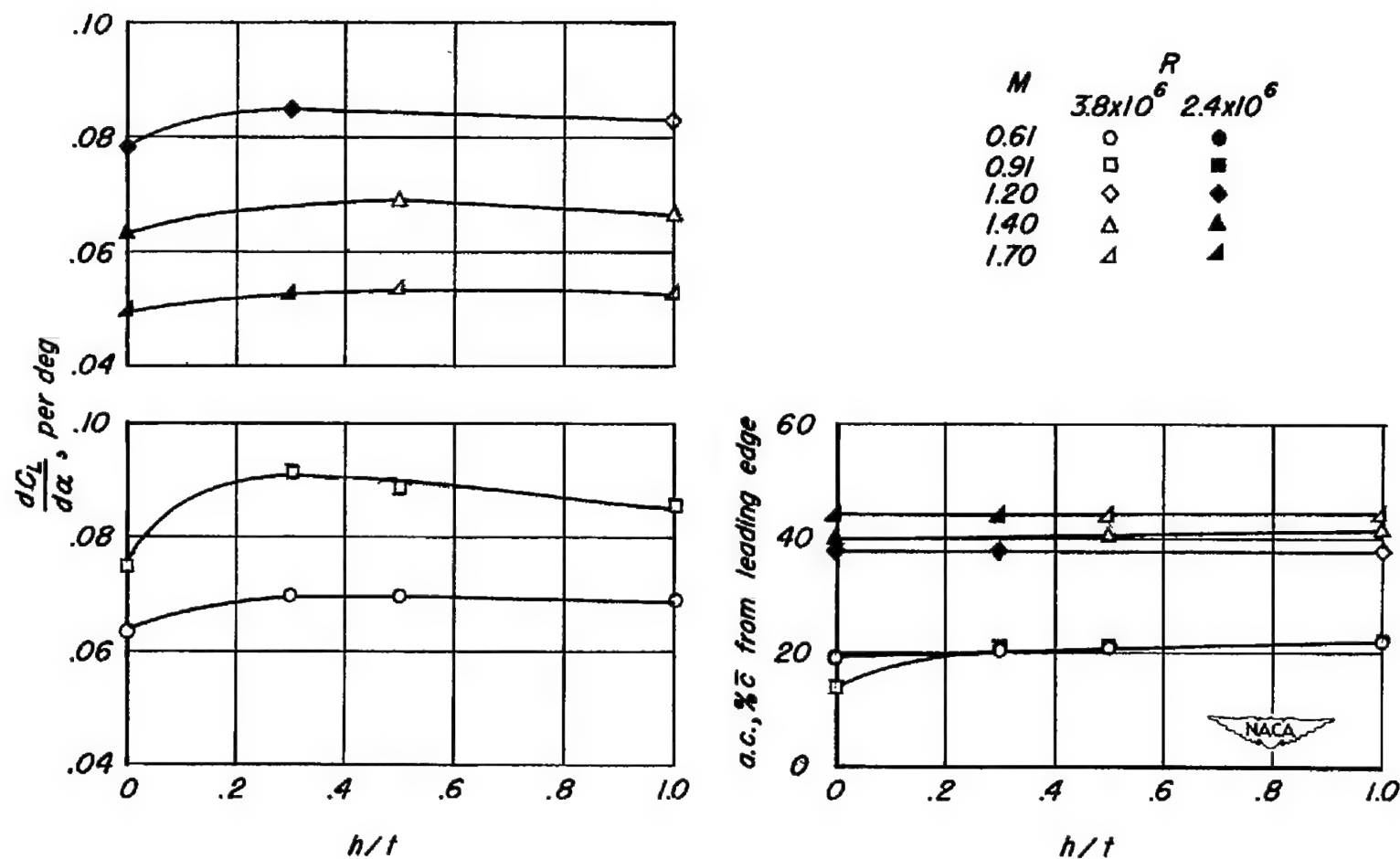


Figure 9.- Variation of lift-curve slope and aerodynamic center of the sharp-nose airfoil with trailing-edge thickness parameter, h/t .

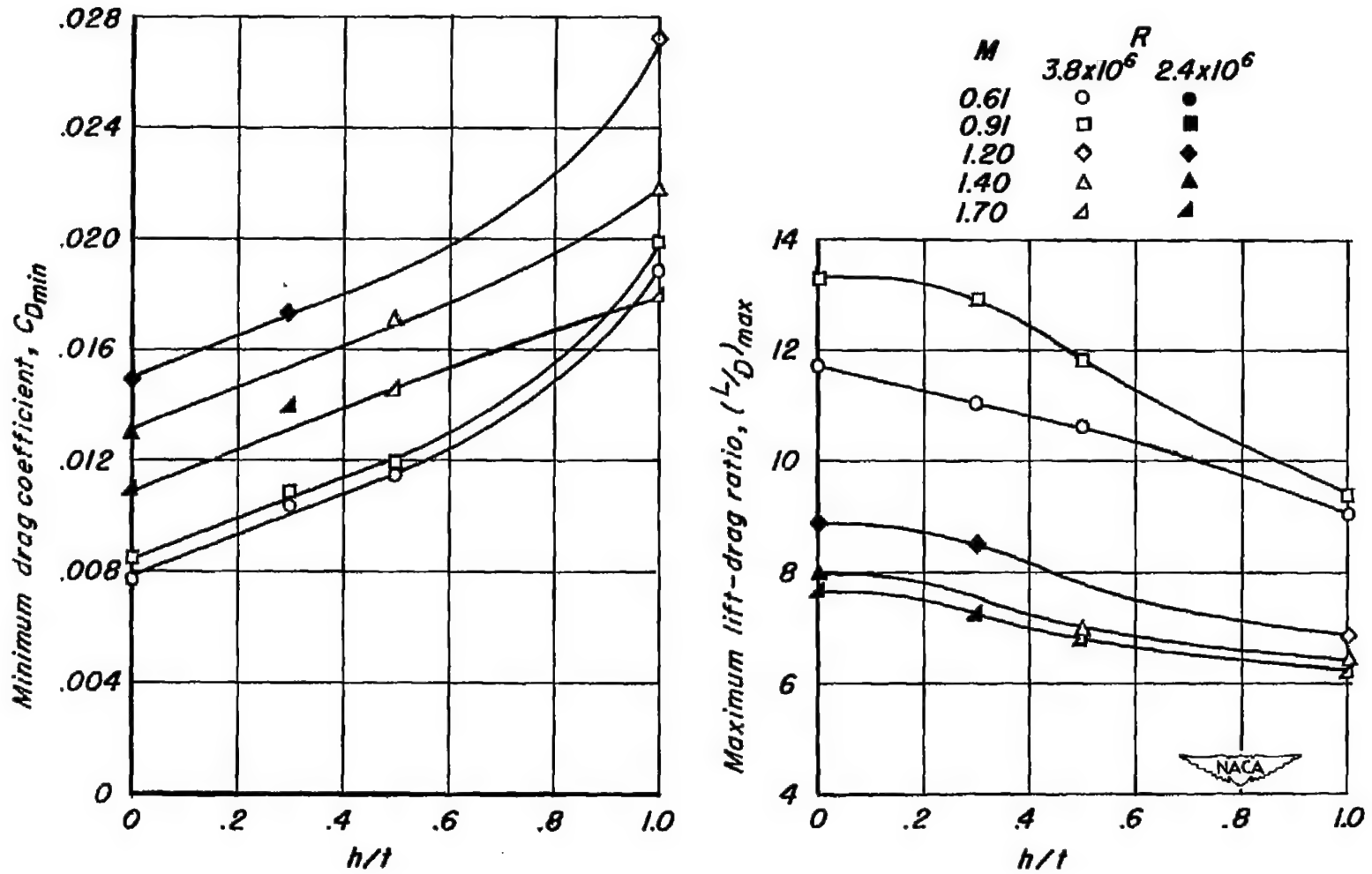
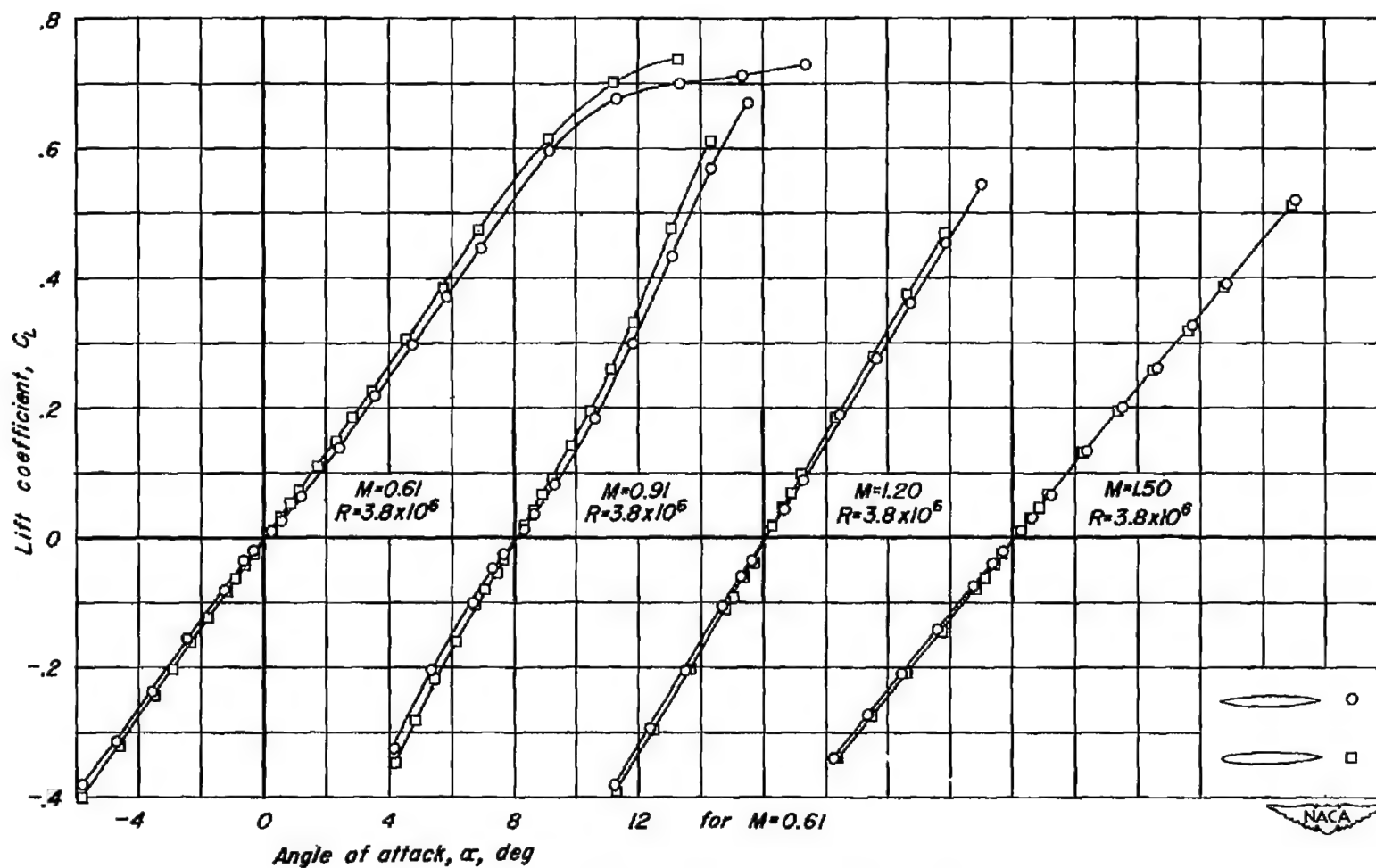
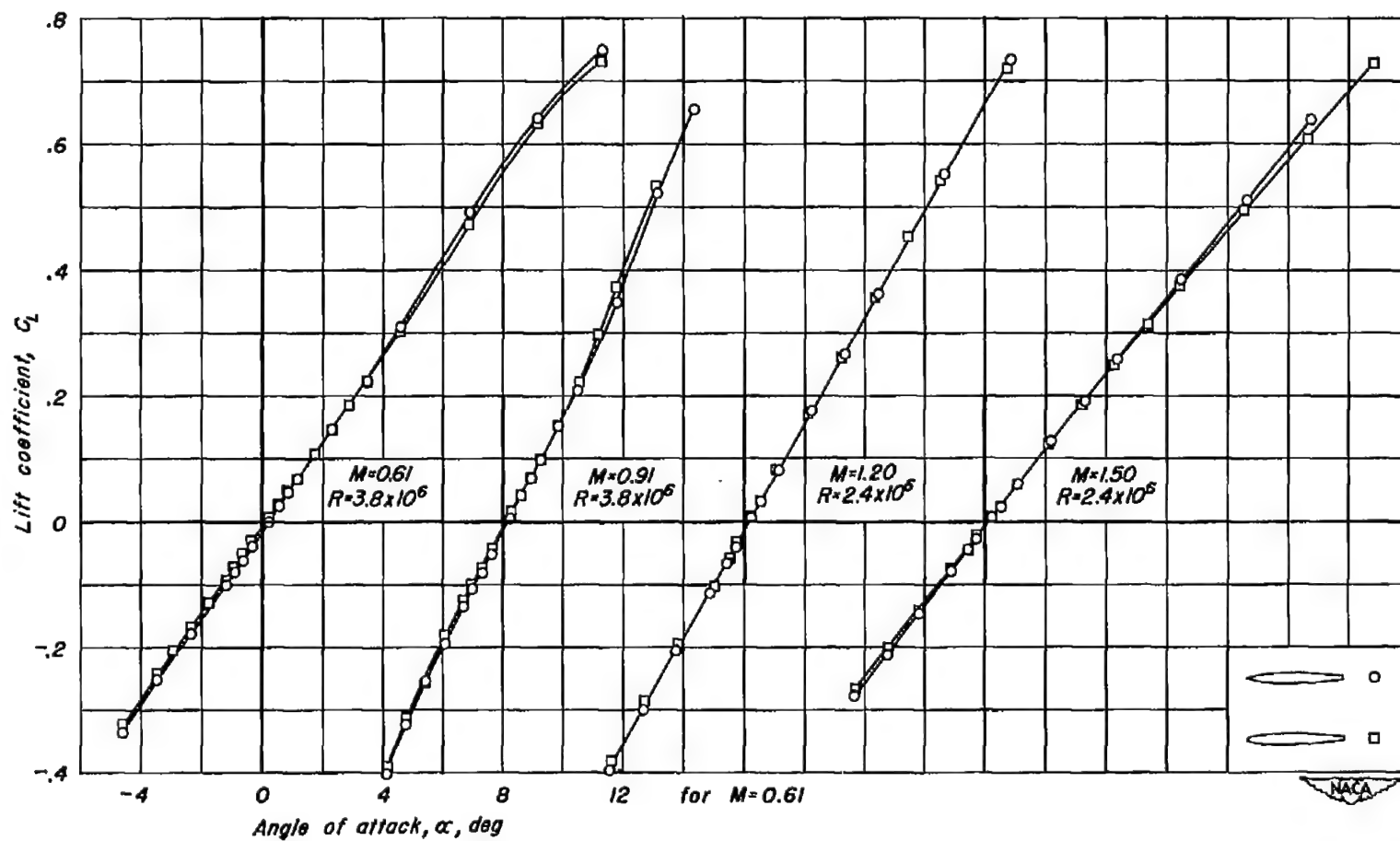


Figure 10.- Variation of minimum drag coefficient and maximum lift-drag ratio of the sharp-nose airfoil with trailing-edge thickness parameter, h/t .



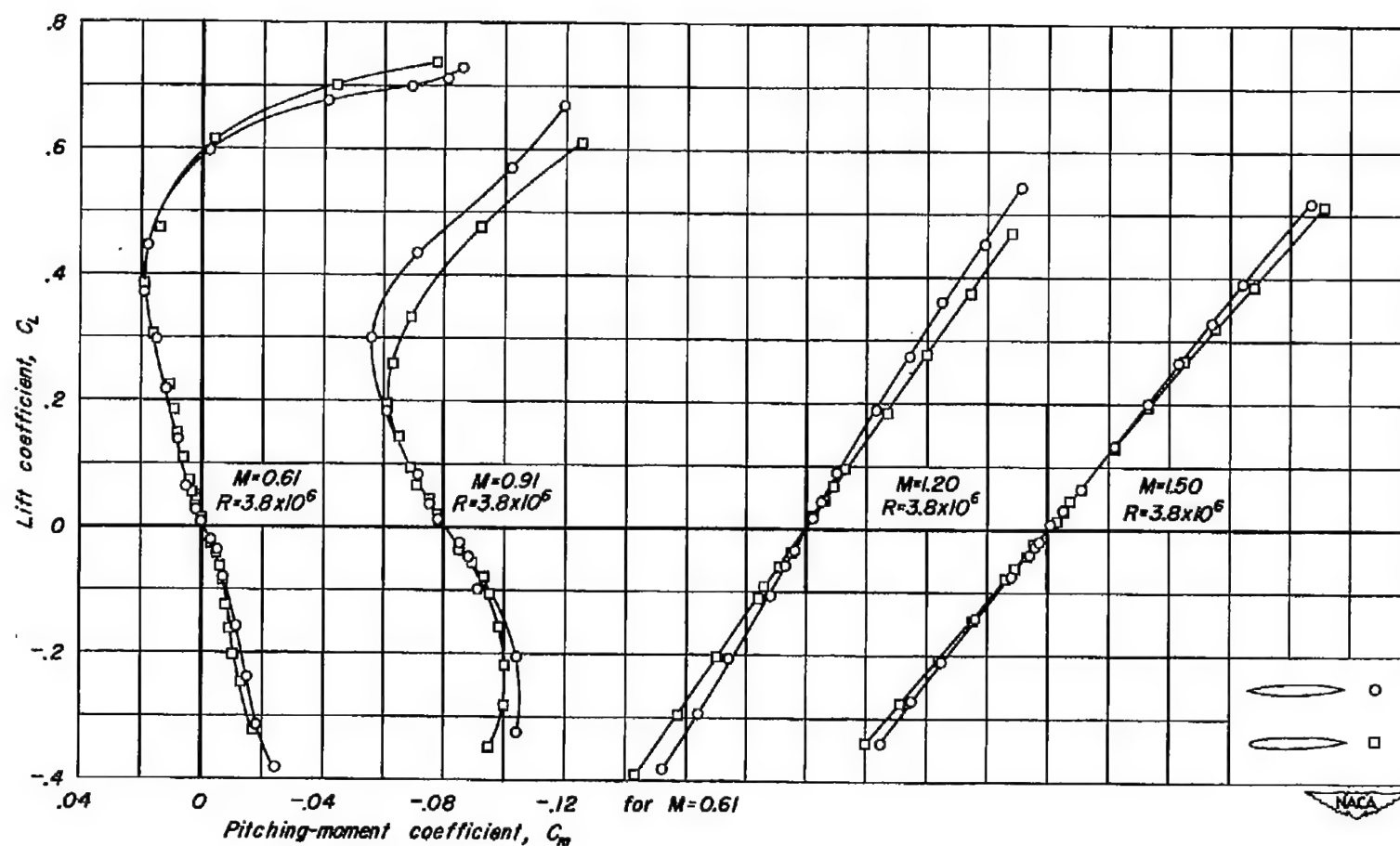
(a) Sharp-trailing-edge airfoils.

Figure 11.- Effect of rounding the section leading edge on the variation of lift coefficient with angle of attack.



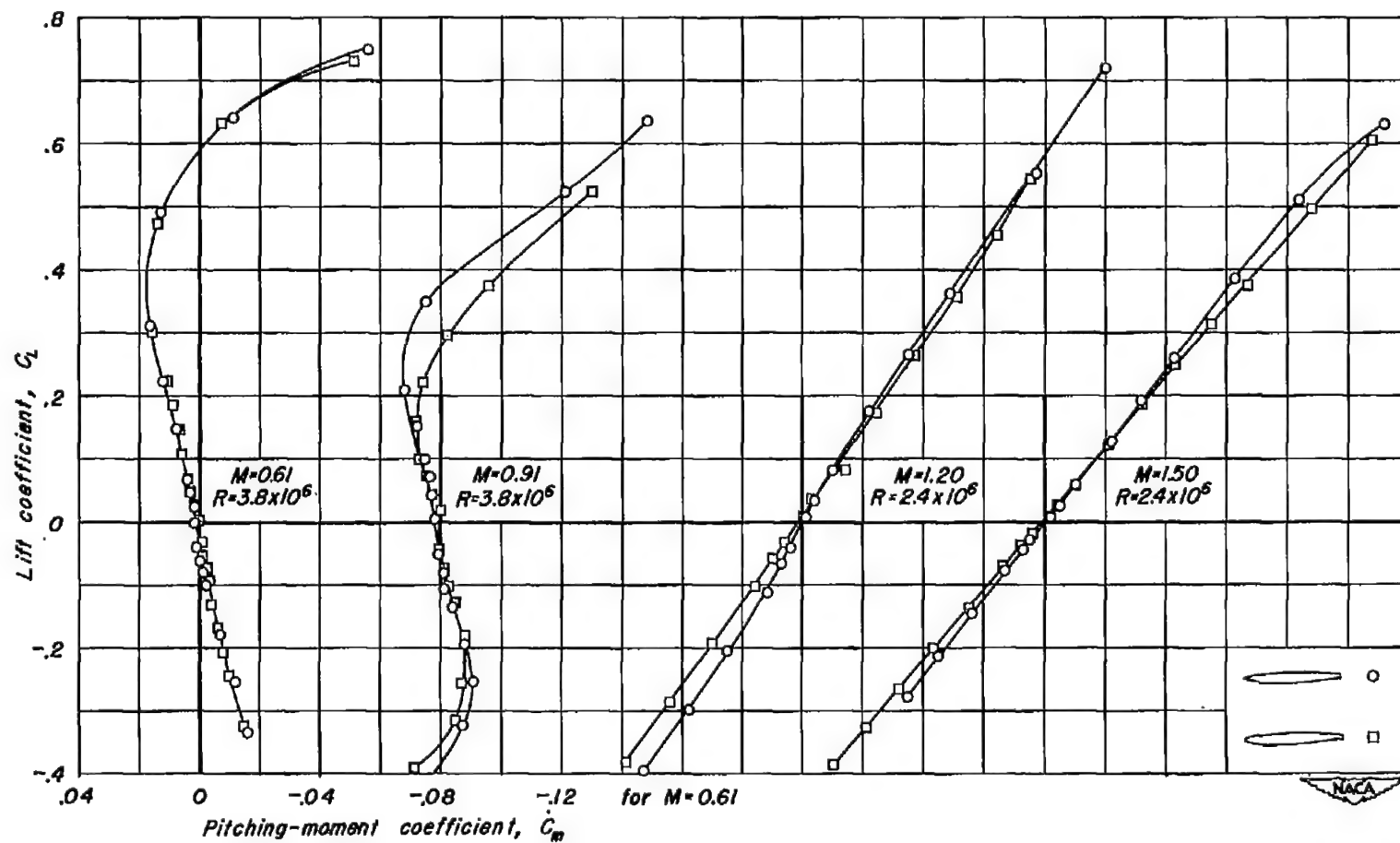
(b) Blunt-trailing-edge airfoils.

Figure 11.- Concluded.



(a) Sharp-trailing-edge airfoils.

Figure 12.- Effect of rounding the section leading edge on the variation of pitching-moment coefficient with lift coefficient.



(b) Blunt-trailing-edge airfoils.

Figure 12.- Concluded.

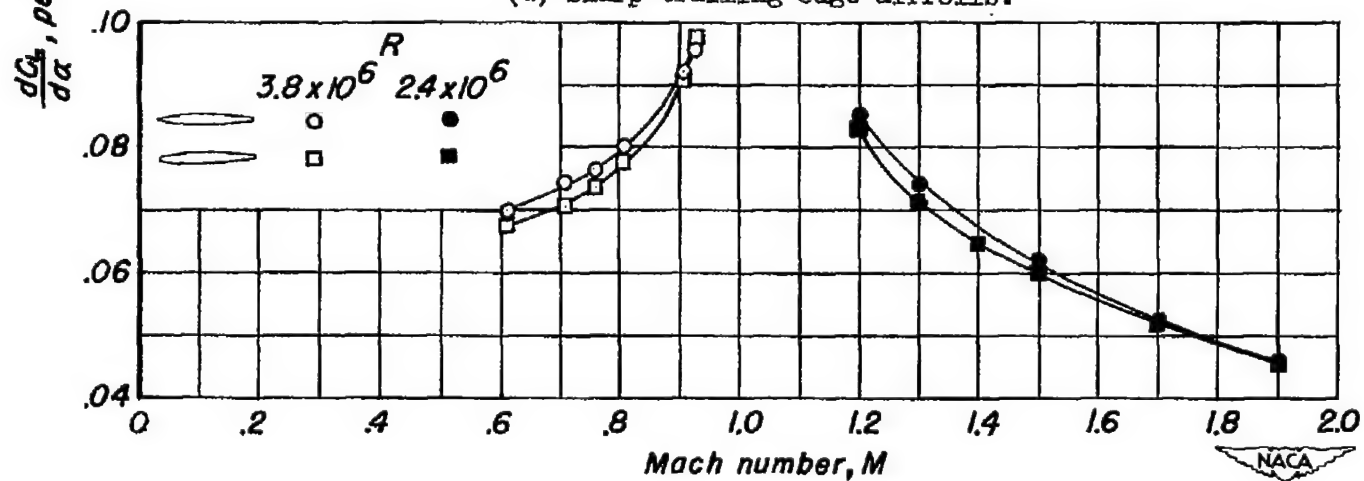
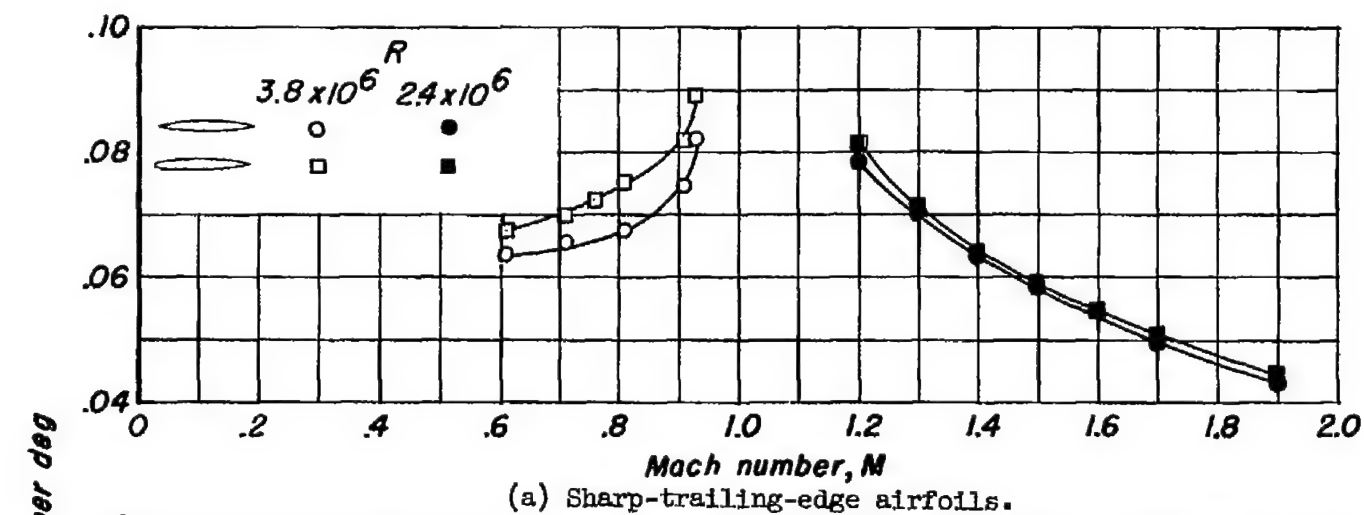
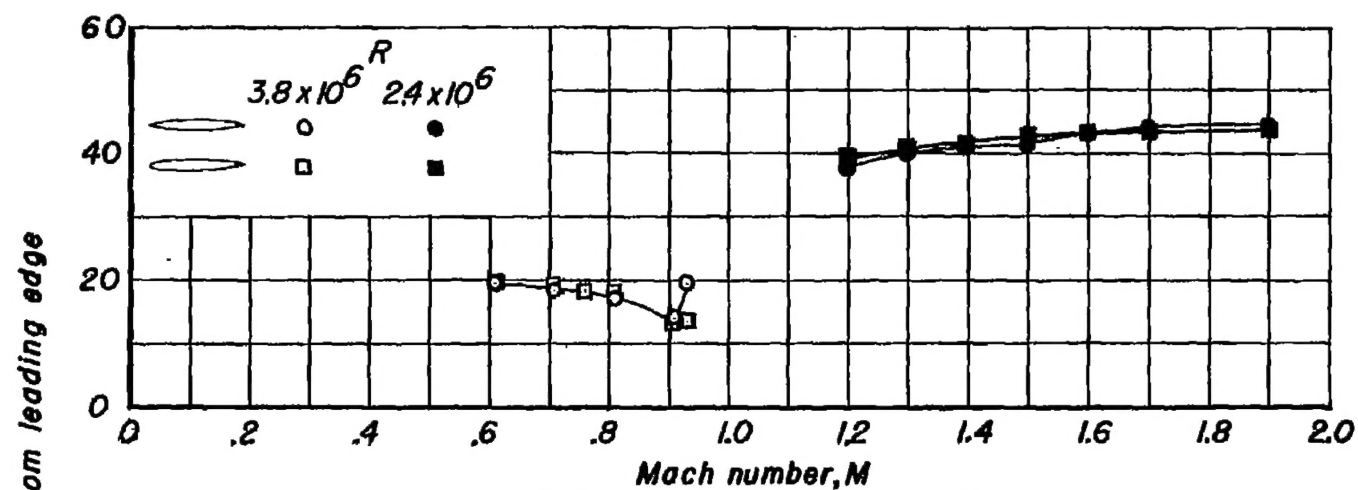
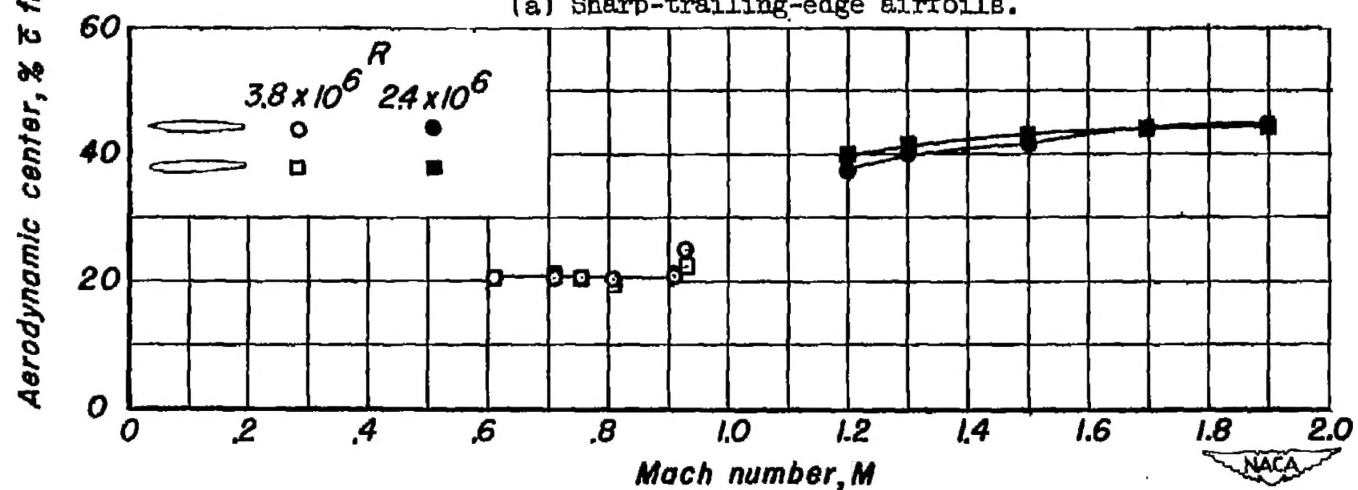


Figure 13.- Effect of rounding the section leading edge on the variation of lift-curve slope with Mach number.

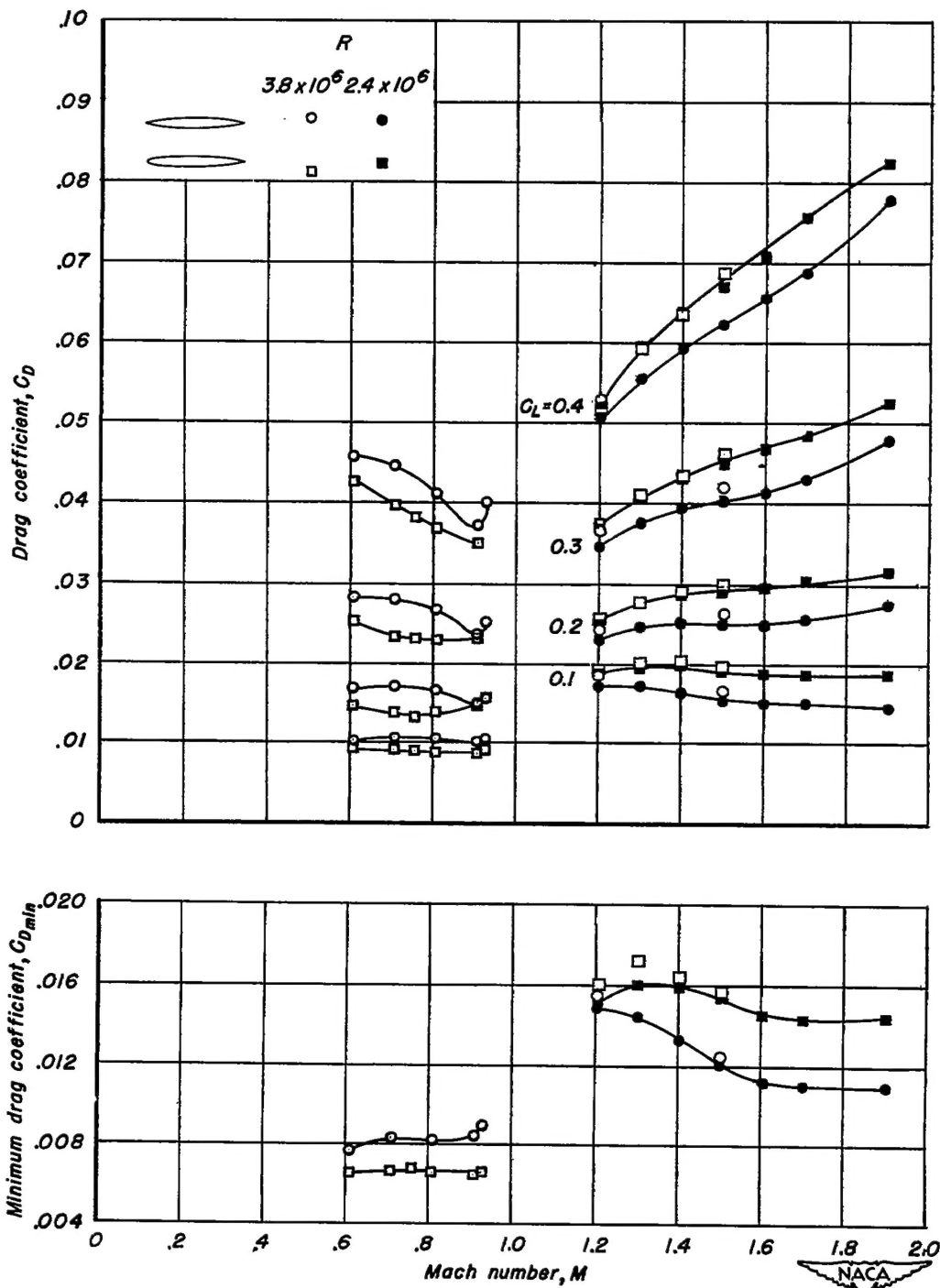


(a) Sharp-trailing-edge airfoils.



(b) Blunt-trailing-edge airfoils.

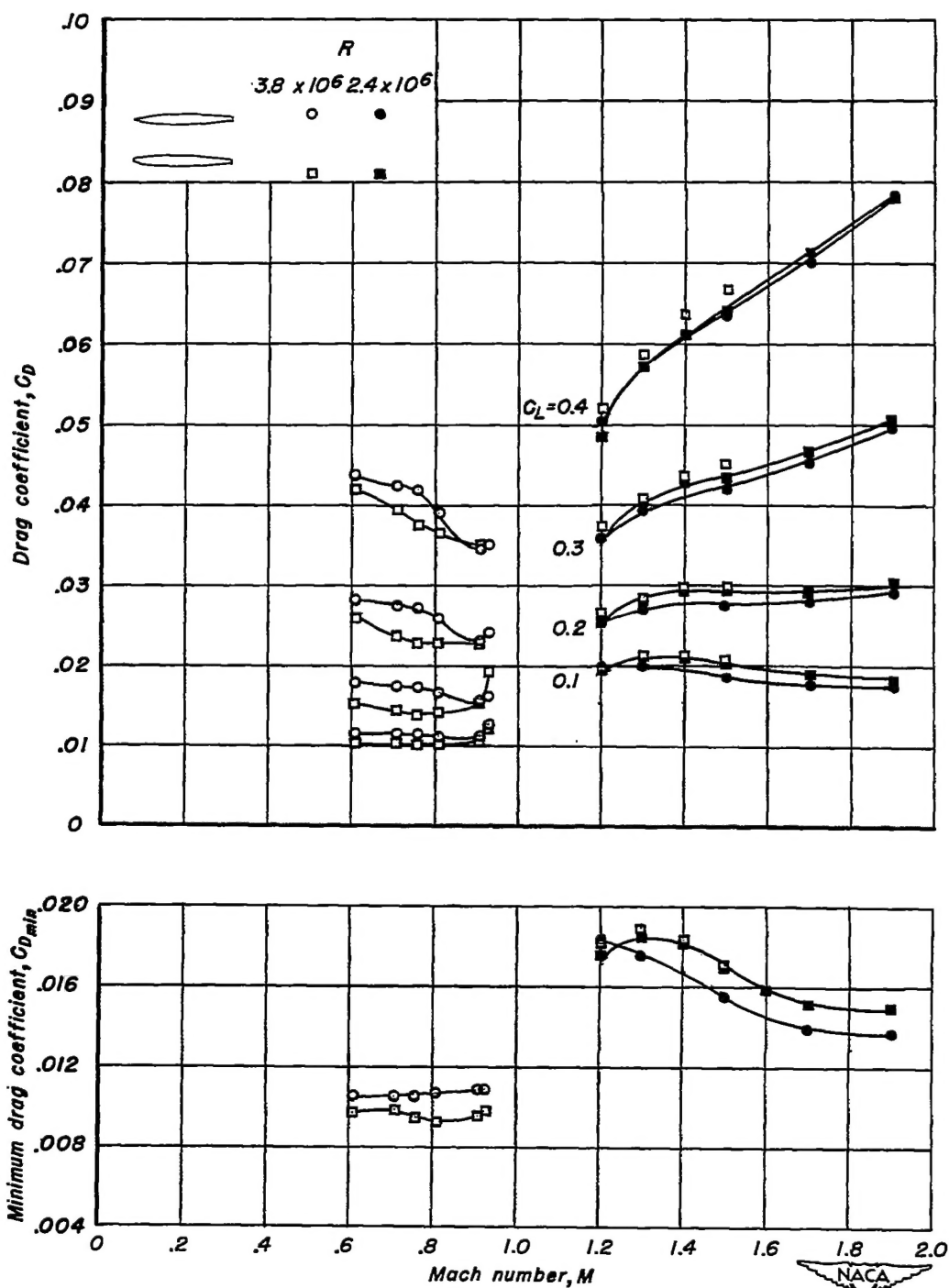
Figure 14.- Effect of rounding the section leading edge on the variation of aerodynamic center with Mach number.

~~CONFIDENTIAL~~

(a) Sharp-trailing-edge airfoils.

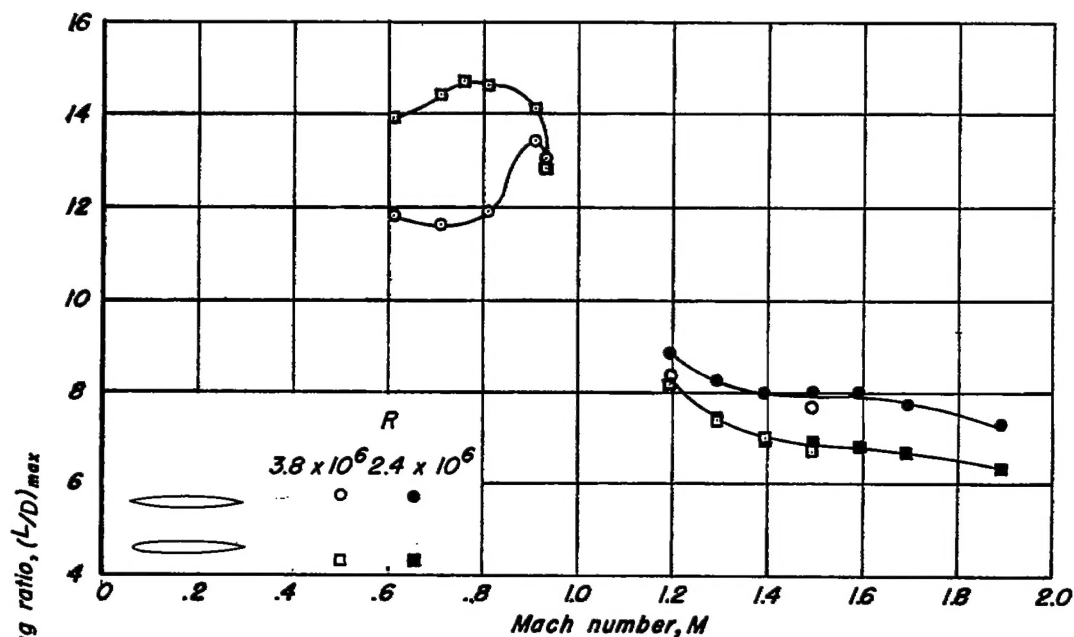
Figure 15.- Effect of rounding the section leading edge on the variation of drag coefficient at various lift coefficients with Mach number.

~~CONFIDENTIAL~~

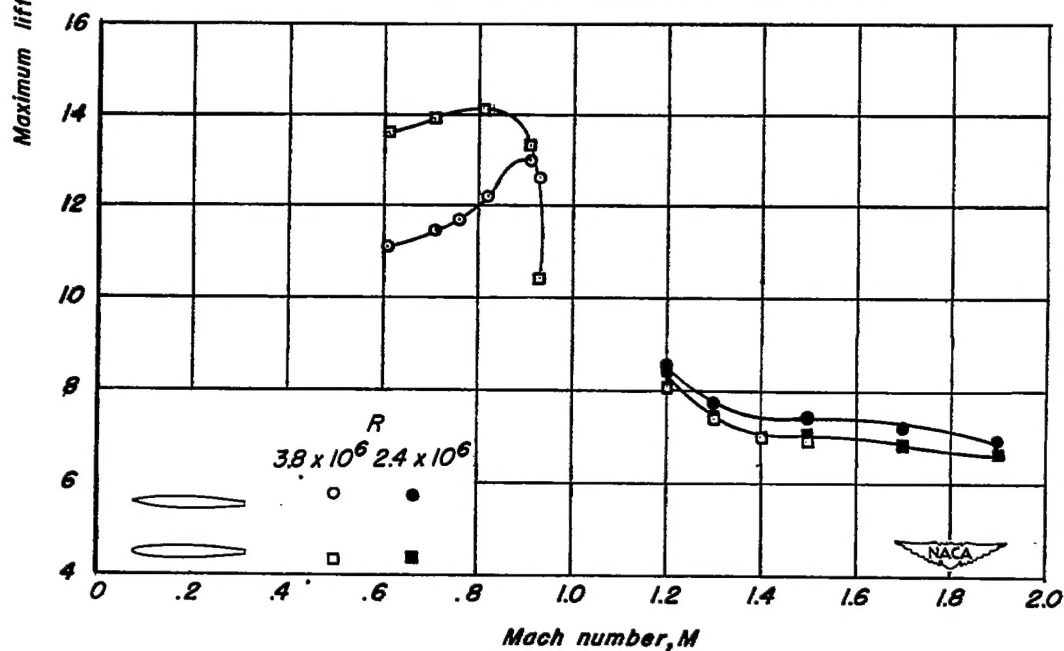


(b) Blunt-trailing-edge airfoils.

Figure 15.- Concluded.



(a) Sharp-trailing-edge airfoils.



(b) Blunt-trailing-edge airfoils.

Figure 16 - Effect of rounding the section leading edge on the variation of maximum lift-drag ratio with Mach number.

